

# Iron(II) Complexes of the Linear *rac*-Tetraphos-1 Ligand as Efficient Homogeneous Catalysts for Sodium Bicarbonate Hydrogenation and Formic Acid Dehydrogenation

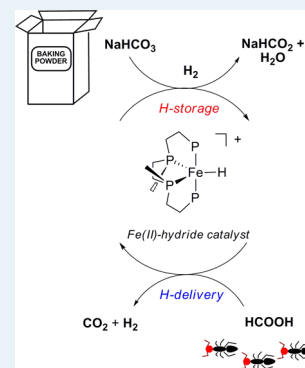
Federica Bertini, Irene Mellone, Andrea Ienco, Maurizio Peruzzini, and Luca Gonsalvi\*

Consiglio Nazionale delle Ricerche, Istituto di Chimica dei Composti Organometallici (CNR-ICCOM), Via Madonna del Piano 10, 50019 Sesto Fiorentino (Firenze), Italy

Supporting Information

**ABSTRACT:** The linear tetraphosphine 1,1,4,7,10,10-hexaphenyl-1,4,7,10-tetraphosphadecane (tetraphos-1, P4) was used as its *rac* and *meso* isomers for the synthesis of both molecularly defined and in situ formed Fe(II) complexes. These were used as precatalysts for sodium bicarbonate hydrogenation to formate and formic acid dehydrogenation to hydrogen and carbon dioxide with moderate to good activities in comparison to those for literature systems based on Fe. Mechanistic details of the reaction pathways were obtained by NMR and HPNMR experiments, highlighting the role of the Fe(II) monohydrido complex  $[\text{FeH}(\text{rac-P4})]^+$  as a key intermediate. X-ray crystal structures of different complexes bearing *rac*-P4 were also obtained and are described herein.

**KEYWORDS:** iron phosphine complexes, formic acid dehydrogenation, bicarbonate hydrogenation, X-ray crystallography, HPNMR mechanistic studies



## INTRODUCTION

Hydrogen is of crucial importance in the chemical industry and holds great potential as a secondary energy carrier, as a feedstock for direct hydrogen fuel cells.<sup>1</sup> Its generation from renewable sources and its storage in a safe and reversible manner are urgent targets for the widespread application of hydrogen in such technologies. Among the different  $\text{H}_2$  storage materials, formic acid (FA) is a nontoxic hydrogen source which can be handled and transported easily and possesses a relatively high  $\text{H}_2$  content (4.4 wt %).  $\text{H}_2$  generation from formic acid affords  $\text{H}_2 + \text{CO}_2$  mixtures and is therefore an "atom efficient" process, since no hydrogen is wasted in the formation of byproducts (such as  $\text{H}_2\text{O}$ , as in the case of  $\text{H}_2$  generation from methanol or methane). In addition, the byproduct  $\text{CO}_2$  can be, in the presence of suitable catalysts, rehydrogenated back to FA, affording a zero-carbon footprint cycle for hydrogen storage and release.<sup>2</sup> The efficient interconversion of FA to  $\text{H}_2$  and  $\text{CO}_2$  is of importance for both  $\text{H}_2$  storage and release and for the utilization of  $\text{CO}_2$  or bicarbonates obtained by its trapping in alkaline water solutions, as a abundant C1 feedstock. In the past decade, there have been a number of reports on selective FA dehydrogenation to produce CO-free  $\text{H}_2$ , as well as on the hydrogenation of  $\text{CO}_2$  or bicarbonates to FA or formate salts. However, most of these catalysts are based on low-abundance noble metals such as ruthenium<sup>3</sup> and iridium.<sup>4</sup> Only recently has this chemistry been extended to non-noble metals such as Fe<sup>5</sup> and Co.<sup>6</sup>

The most active additive-free Fe-based catalyst system for FA dehydrogenation under mild temperature conditions (40 °C) reported to date was obtained by combining the iron(II) salt  $\text{Fe}(\text{BF}_4)_2 \cdot 6\text{H}_2\text{O}$  with the tetraphosphine ligand  $\text{P}(\text{CH}_2\text{CH}_2\text{PPh}_2)_3$  ( $\text{PP}_3$ ).<sup>5e,7</sup> Although the nature of the initial complex formed in this reaction has not been fully ascertained, mechanistic studies indicated that under catalytic conditions (FA in propylene carbonate (PC)) complexes  $[\text{FeH}(\text{PP}_3)]^+$  and  $[\text{FeH}(\eta^2\text{-H}_2)(\text{PP}_3)]^+$  are formed.<sup>5e,8</sup> This catalytic system was successfully applied to bicarbonate hydrogenation to formates and carbon dioxide valorization to alkyl formates and formamides.<sup>5a</sup> In continuation of this work, efficient iron-catalyzed hydrogenation of carbon dioxide and bicarbonates was achieved using  $\text{Fe}(\text{BF}_4)_2 \cdot 6\text{H}_2\text{O}$  and  $\text{P}^{\text{Ph}}\text{P}_3$  ( $\text{P}^{\text{Ph}}\text{P}_3 = \text{tris}(2\text{-diphenylphosphino)phenylphosphine}$ ). In this case, metal complexation afforded the well-defined complex  $[\text{FeF}(\text{P}^{\text{Ph}}\text{P}_3)]^+$  via F-BF<sub>3</sub> activation. Mechanistic studies established that this complex reacts with  $\text{H}_2$  to give  $[\text{FeH}(\eta^2\text{-H}_2)(\text{P}^{\text{Ph}}\text{P}_3)]^+$ . High-pressure HPNMR  $\text{CO}_2$  hydrogenation experiments in the presence of  $\text{NEt}_3$  suggested the formation of the known dihydride complex  $[\text{Fe}(\text{H})_2(\text{P}^{\text{Ph}}\text{P}_3)]$ .<sup>5f</sup>

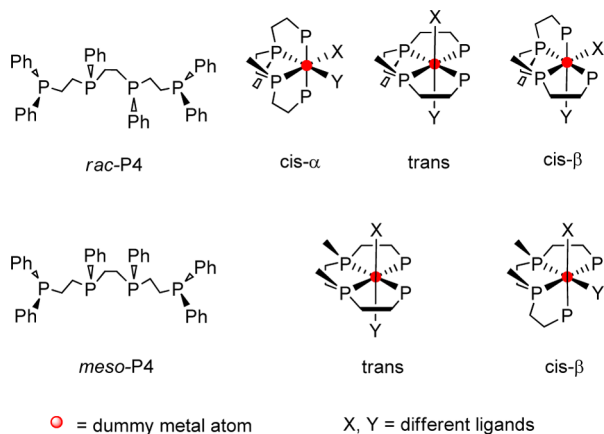
In recent years, our group has been interested in FA dehydrogenation and  $\text{CO}_2$  hydrogenation, so far using Ru<sup>9</sup> and Ir<sup>10</sup> homogeneous catalysts. In an effort to develop novel, non-noble-metal-based catalysts for such transformations, we

Received: September 4, 2014

72 became eager to explore the potential of Fe(II) complexes of  
73 other tetradentate phosphines.

74 The linear tetradentate phosphine ligand 1,1,4,7,10,10-  
75 hexaphenyl-1,4,7,10-tetraphosphadecane (tetraphos-1, P4) ex-  
76 ists as a mixture of *rac* (*S,S;R,R*) and *meso* (*S,R*)  
77 diastereoisomers (hereafter *rac*-P4 and *meso*-P4, respectively),  
78 which can be separated by fractional crystallization.<sup>11,12</sup> Despite  
79 the fact that the existence of these stereoisomers was  
80 recognized as early as 1974,<sup>13</sup> the importance of this isomerism  
81 was not fully appreciated until the work of Brown and  
82 Canning.<sup>11</sup> The configurations that these diastereoisomers can  
83 adopt in an octahedral complex are denoted as *cis-α*, *cis-β*, and  
84 *trans* (Chart 1). While the *meso* isomer can adopt only a *trans*

Chart 1. *rac* and *meso* Isomers of tetraphos-1 (P4) and Allowed Configurations for Their Octahedral Complexes



85 or *cis-β* configuration, all three configurations are physically  
86 possible for the *rac* isomer. Nevertheless, the *rac* isomer is  
87 known for its propensity to form *cis-α* complexes.<sup>11,14</sup> Since the  
88 original preparation of tetraphos-1 by King and co-workers,<sup>15</sup>  
89 there have been a number of reports on its coordination  
90 behavior.<sup>11–16</sup> By a close perusal of the available literature, we  
91 noticed that the chemistry of the *meso* isomer is far more  
92 developed than that of the *rac* isomer. Only complexes  
93  $[\text{FeBr}(\text{P4})][\text{BPh}_4]$ <sup>16d</sup> and  $\text{trans-}[\text{FeH}(\text{N}_2)(\text{P4})]$ <sup>16c</sup> have been  
94 characterized crystallographically, and in both the ligand  
95 exhibits a *meso* configuration. This was probably due to the  
96 fact that the authors used commercial tetraphos-1, which is  
97 richer in the *meso* isomer. The syntheses of  $[\text{FeH}(\text{P4})]\text{X}$ ,  
98  $[\text{Fe}(\text{NCS})_2(\text{P4})]$ ,  $[\text{FeH}(\text{NCS})(\text{P4})]\text{X}$ , and  $[\text{FeH}(\text{CO})(\text{P4})]$   
99 ( $\text{X} = \text{Br}, \text{I}$ ) were also described, but no indication of the  
100 configuration of the P4 ligand was provided.<sup>16e</sup> Morris and co-  
101 workers reported on the hydrogen exchange between  $\eta^2\text{-H}_2$  and  
102 hydride ligands in  $\text{trans-}[\text{FeH}(\eta^2\text{-H}_2)(\text{meso-P4})]\text{BF}_4$ , obtained  
103 by protonation of the corresponding dihydride complex  $\text{trans-}$   
104  $[\text{Fe}(\text{H})_2(\text{meso-P4})]$ .<sup>12,14</sup> To the best of our knowledge, a full  
105 exploration of the coordination chemistry of *rac*-P4 to Fe(II)  
106 and the reactivity of the complexes so obtained has never been  
107 reported.

108 In this work, we describe the synthesis of novel Fe(II)  
109 complexes bearing *rac*-P4, their reactivity toward  $\text{H}_2$  and  $\text{CO}_2$ ,  
110 and their application as efficient catalysts for FA dehydrogen-  
111 ation and sodium bicarbonate hydrogenation to sodium  
112 formate. The catalytic data are complemented by mechanistic  
113 details obtained by model stoichiometric reactions and in  
114 operando high-pressure HPNMR experiments.

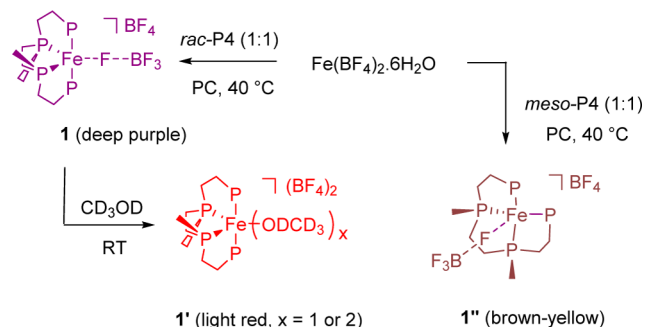
## RESULTS AND DISCUSSION

115

### Syntheses and Characterization of Fe(II) Complexes.

116 At first, *rac*-P4 and *meso*-P4 were obtained in pure isomeric  
117 form from the commercial ligand P4, containing a *rac:meso*  
118 ratio of 1:3, by fractional crystallization as described in the  
119 literature.<sup>14</sup> In order to test the coordination abilities of the two  
120 isomers with suitable iron(II) sources, the commercially  
121 available salt  $\text{Fe}(\text{BF}_4)_2 \cdot 6\text{H}_2\text{O}$  and the easily accessible  
122 complex<sup>17</sup>  $[\text{Fe}(\text{CH}_3\text{CN})_6](\text{BF}_4)_2$  were used as metal precursors.  
123 The reaction of  $\text{Fe}(\text{BF}_4)_2 \cdot 6\text{H}_2\text{O}$  with *rac*-P4 (1:1) was  
124 rather sluggish in a variety of common solvents, whereas it  
125 proceeded smoothly in propylene carbonate (PC), affording a  
126 deep purple solution. The  $^{31}\text{P}\{^1\text{H}\}$  NMR spectrum of this  
127 solution ( $\text{C}_6\text{D}_6$  insert) showed two broad signals at  $\delta_{\text{p}}$  99.9 and  
128 60.9 ppm, indicative of Fe(II) complexation by the ligand.  
129  $^{19}\text{F}\{^1\text{H}\}$  NMR analysis at room temperature showed only a  
130 single, sharp peak for the  $\text{BF}_4$  anion, suggesting that the  
131 complex  $[\text{FeF}(\text{rac-P4})](\text{BF}_4)$ , expected to arise upon F– $\text{BF}_3$   
132 bond activation,<sup>5f</sup> had not formed. Due to the known  
133 propensity of Fe(P4) complexes to adopt a pentacoordinate  
134 geometry, often completed by halide ligands,<sup>16c,d,f</sup> we propose  
135 that under these conditions the complex  $[\text{Fe}(\eta^1\text{-F}(\text{BF}_3))(\text{rac-}$   
136  $\text{P4})](\text{BF}_4)$  (**1**) has formed, where one of the  $\text{BF}_4$  counterions  
137 acts as a weakly coordinating ligand (Scheme 1).<sup>18</sup> This  
138 s1

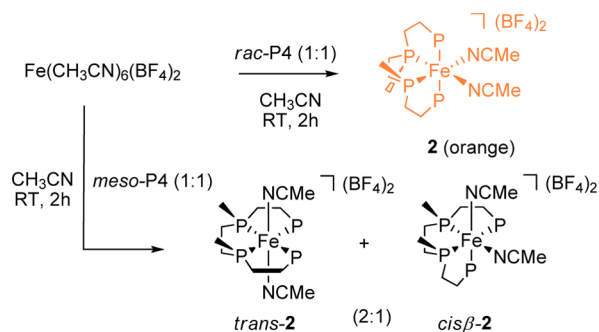
Scheme 1. Reactivity of  $\text{Fe}(\text{BF}_4)_2 \cdot 6\text{H}_2\text{O}$  with *rac*-P4 and *meso*-P4 to give **1**, **1'**, and **1''**



139 complex is likely to be fluxional in solution, and the loosely  
140 bound  $\text{BF}_4$  can be easily replaced by a coordinating solvent X  
141 ( $\text{X} = \text{H}_2\text{O}, \text{MeOH}$ ),<sup>19</sup> giving complexes such as *cis-α*-  
142  $[\text{FeX}_2(\text{rac-P4})](\text{BF}_4)_2$ . This was proven by addition of  
143  $\text{CD}_3\text{OD}$  to a solution of **1** in PC, where a new species formed,  
144 showing a  $^{31}\text{P}\{^1\text{H}\}$  NMR pattern composed of two triplets at  $\delta_{\text{p}}$   
145 107.6 and 73.8 ( $^2J_{\text{PP}} = 29.9$  Hz), which we attribute to the  
146 solvento species *cis-α*- $[\text{Fe}(\text{CD}_3\text{OD})_x(\text{rac-P4})](\text{BF}_4)_2$  (**1'**;  $x = 1,$   
147 2). To date, all our attempts to obtain crystals of either **1** or **1'**  
148 failed. A similar reactivity was observed upon reacting  
149  $\text{Fe}(\text{BF}_4)_2 \cdot 6\text{H}_2\text{O}$  with *meso*-P4, which resulted in the formation  
150 of a brown solution containing the putative complex  $[\text{Fe}(\eta^1\text{-}$   
151  $\text{F}(\text{BF}_3))(\text{meso-P4})](\text{BF}_4)$  (**1''**), also characterized by two broad  
152 signals in the  $^{31}\text{P}\{^1\text{H}\}$  NMR at  $\delta_{\text{p}}$  104.8 and 70.8 ppm.

153 In contrast, the reaction of *rac*-P4 with  $[\text{Fe}(\text{CH}_3\text{CN})_6]\text{BF}_4$   
154 resulted in the quantitative formation of the well-defined  
155 complex *cis-α*- $[\text{Fe}(\text{CH}_3\text{CN})_2(\text{rac-P4})](\text{BF}_4)_2$  (**2**) as the sole  
156 s2 product (Scheme 2). The  $^{31}\text{P}\{^1\text{H}\}$  NMR spectrum exhibits two  
157 triplets at 100.7 and 65.6 ppm in  $\text{CD}_3\text{CN}$ , which reflect an  
158 AA'XX' coupling pattern with equivalent *cis*-P,P coupling  
159 constants ( $^2J_{\text{PP}} = 31.7$  Hz). These values are in close analogy  
160 with those attributed by Habeck et al. to *cis-α*- $[\text{Fe}$   
161  $(\text{NCS})_2(\text{rac-P}^i\text{P4})]$  ( $\text{rac-P}^i\text{P4} = 1,1,4,8,11,11\text{-hexaphenyl-}$

**Scheme 2. Synthesis of *rac*-P4 and *meso*-P4 Complexes Starting from  $[\text{Fe}(\text{CH}_3\text{CN})_6](\text{BF}_4)_2$ .**



162 1,4,8,11-tetraphosphaundecane).<sup>20</sup> Crystals suitable for X-ray  
163 diffraction analysis were grown by adding *n*-pentane to a  
164 solution of **2** in acetonitrile/methanol (Figure 1). Complex **2**

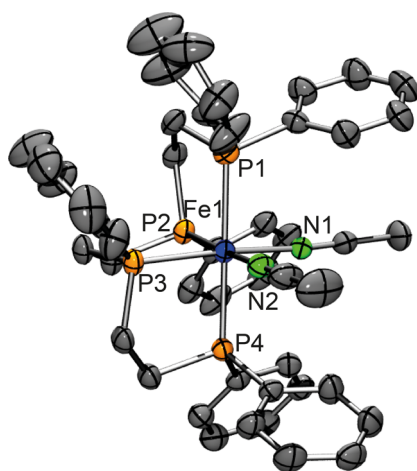


**Figure 1.** Molecular structure for the cationic portion of **2**. Ellipsoids are set at the 50% probability level. Hydrogen atoms are omitted for clarity. Selected bond lengths (Å) and bond angles (deg): Fe1–N1, 1.943(3); Fe1–N2, 1.955(4); Fe1–P1, 2.2869(13); Fe1–P2, 2.2137(12); Fe1–P3, 2.2246(12); Fe1–P4, 2.2981(13); N1–Fe1–N2, 88.70(15); N1–Fe1–P1, 90.36(11); N1–Fe1–P2, 92.50(11); N1–Fe1–P3, 174.50(12); N1–Fe1–P4, 90.06(11); N2–Fe1–P1, 91.57(12); N2–Fe1–P2, 117.12(12); N2–Fe1–P3, 93.76(11); N2–Fe1–P4, 88.25(12).

165 crystallizes in the  $C2/c$  space group and has an octahedral  
166 coordination geometry at the Fe(II) center, with Fe– $P_{ax}$   
167 distances (Fe1–P1 = 2.2868(13) Å and Fe1–P4 =  
168 2.2982(13) Å) that are longer than the Fe– $P_{eq}$  distances  
169 (Fe1–P2 2.2138(13) and Fe1–P3 2.2247(12) Å). Notably,  
170 complex **2** was stable in air as a solid and solutions in  
171 acetonitrile/methanol could be stored under nitrogen for over  
172 1 month without any appreciable decomposition. In contrast,  
173 the reaction of *meso*-P4 with  $[\text{Fe}(\text{CH}_3\text{CN})_6](\text{BF}_4)_2$  was not  
174 selective and afforded a mixture of two products in an  
175 approximately 2:1 ratio, which were identified on the basis of  
176 characteristic  $^{31}\text{P}\{^1\text{H}\}$  NMR resonances<sup>12,20</sup> (see the [Supporting](#)  
177 [Information](#)) as the *trans*- and *cis*- $\beta$  isomers of  $[\text{Fe}$   
178  $(\text{CH}_3\text{CN})_2(\text{meso-P4})](\text{BF}_4)_2$ , respectively.

179 **Syntheses of Fe(*rac*-P4) Hydrido Complexes.** Due to  
180 the relevance of Fe–hydrido complexes to FA dehydrogenation  
181 and bicarbonate hydrogenation reactions, we targeted the  
182 syntheses of the so far unknown mono- and dihydride iron

complexes of *rac*-P4. The analogues of the *meso* isomer have 183  
been previously reported.<sup>12,16e</sup> The monohydrido complex 184  
 $[\text{FeH}(\text{rac-P4})][\text{BPh}_4]$  (**3-BPh<sub>4</sub>**) was obtained upon reacting 185  
*rac*-P4, anhydrous  $\text{FeCl}_2$ ,  $\text{NaBPh}_4$ , and  $\text{NaBH}_4$  in stoichio- 186  
metric amounts in THF/MeOH and was characterized by 187  
NMR and X-ray diffraction studies upon growing suitable 188  
crystals from these solutions. The  $^{31}\text{P}\{^1\text{H}\}$  NMR spectrum of 189  
**3-BPh<sub>4</sub>** in  $d_8$ -THF showed two triplets at  $\delta_p$  119.4 and 99.4 190  
ppm, reflecting an AA'XX' coupling pattern with an observed 191  
splitting of 24.5 Hz, while in the corresponding  $^1\text{H}$  NMR 192  
spectrum, the hydride signal appeared as a broad triplet at 193  
–9.16 ppm ( $^2J_{\text{HP}} = 24.0$  Hz). The crystal structure of **3-BPh<sub>4</sub>** 194  
displays a pseudo-octahedral geometry, with the hydride ligand 195  
occupying two sites in the crystal: i.e., alternatively one or the 196  
other *cis* position in 50% occupancy (Figure 2). The distortion 197  $\Omega$

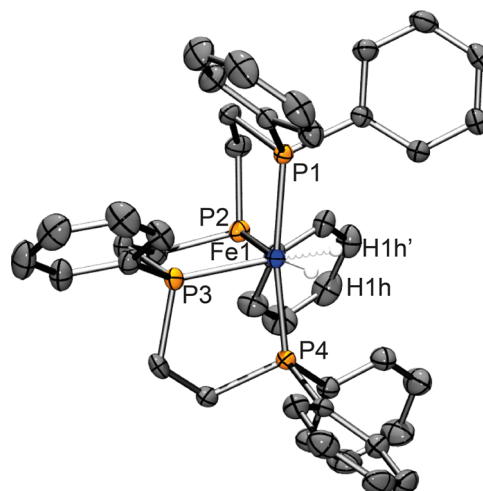


**Figure 2.** Molecular structure for the cationic portion of **3-BPh<sub>4</sub>**. Ellipsoids are set at the 50% probability level. Hydrogen atoms are omitted for clarity, except for the hydride ligand. Selected bond lengths (Å) and bond angles (deg): Fe1–P1, 2.2189(7); Fe1–P2, 2.1961(7); Fe1–P3, 2.2207(7); Fe1–P4, 2.1993(8); Fe1–H1h, 1.61(5); Fe1–H1h', 1.41(5); H1h–Fe1–H1h', 90(3); P1–Fe1–P2, 85.38(3); P1–Fe1–P3, 102.58(3); P1–Fe1–P4, 170.41(3); P2–Fe1–P3, 85.74(3); P2–Fe1–P4, 96.87(3); P3–Fe1–P4, 86.91(3); H1h–Fe1–P1, 89.0(2); H1h–Fe1–P2, 172.4(18); H1h–Fe1–P3, 100.6(18); H1h–Fe1–P4, 87(2); H1h'–Fe1–P1, 83(2); H1h'–Fe1–P2, 83(2); H1h'–Fe1–P3, 168(2); H1h'–Fe1–P4, 87(2).

from the ideal octahedral geometry is evident from the P1– 198  
Fe1–P4 angle (170.4°), which is significantly bent in 199  
comparison to the analogous P1–Fe1–P4 angle in **2** 200  
(179.5°), whereas the P2–Fe1–P3 angles are comparable in 201  
**2** and **3** (85.3° vs 85.7°). 202

The neutral dihydrido complex *cis*- $\alpha$ - $[\text{Fe}(\text{H})_2(\text{rac-P4})]$  (**4**) 203  
was synthesized from *rac*-P4, anhydrous  $\text{FeCl}_2$ , and excess 204  
 $\text{NaBH}_4$  under reflux conditions in a THF/EtOH mixture. The 205  
 $^{31}\text{P}\{^1\text{H}\}$  NMR spectrum of **4** in  $d_8$ -THF displayed two triplets 206  
at  $\delta_p$  123.8 and 113.1 ppm with  $^2J_{\text{PP}} = 13.5$  Hz due to *cis*-P,P 207  
coupling, whereas the two hydride ligands gave a complex 208  
multiplet centered at –11.7 ppm (apparent double septuplet; 209  
see the [Supporting Information](#)). Crystals of **4** suitable for X- 210  
ray analysis were grown by diffusion of MeOH into the solution 211  
which resulted from the reaction mixture, after filtration and 212  
partial evaporation of the solvent. The solid-state molecular 213  
structure of **4** displays a significantly distorted octahedral 214  
coordination geometry at the Fe(II) center with the *rac*-P4 215  $\Omega$

ligand adopting a *cis-α* configuration (Figure 3). The P1–Fe1–P4 angle in **4** (159.6°) is significantly more distorted than that

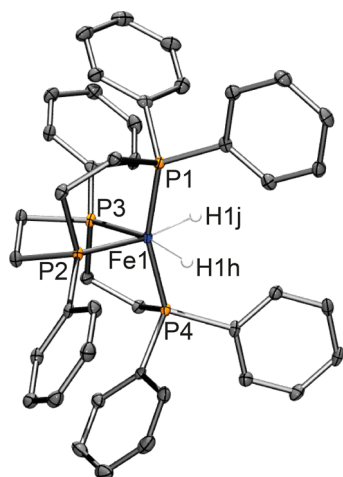


**Figure 3.** Molecular structure of **4**. Ellipsoids are set at the 50% probability level. Hydrogen atoms are omitted for clarity, except for hydrido ligands. Selected bond lengths (Å) and bond angles (deg): Fe1–P1, 2.1249(7); Fe1–P2, 2.1510(7); Fe1–P3, 2.1654(7); Fe1–P4, 2.1303(7); Fe1–H1h, 1.55(3); Fe1–H1j, 1.57(2); H1h–Fe1–H1j, 90.6(13); P1–Fe1–P2, 89.00(3); P1–Fe1–P3, 106.14(3); P1–Fe1–P4, 159.62(3); P2–Fe1–P3, 86.05(2); P2–Fe1–P4, 106.21(3); P3–Fe1–P4, 88.71(3); H1h–Fe1–P1, 85.0(9); H1h–Fe1–P2, 91.8(9); H1h–Fe1–P3, 168.6(9); H1h–Fe1–P4, 81.1(9); H1j–Fe1–P1, 82.3(9); H1j–Fe1–P2, 93.3(9); H1j–Fe1–P3, 171.8(9); H1j–Fe1–P4, 83.0(9).

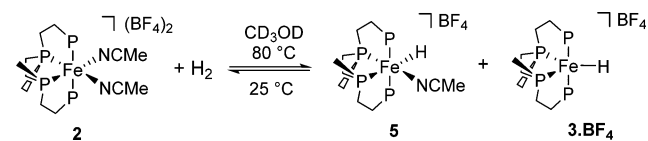
in **3-BPh<sub>4</sub>** (170.4°). Furthermore, all Fe–P bond distances are significantly shorter (all <2.17 Å) with respect to those observed in **2** (2.19–2.22 Å) and **3-BPh<sub>4</sub>** (2.21–2.30 Å).

**Reactivity of 1 and 2 toward H<sub>2</sub>.** To verify the potential of **1** and **2** as hydrogenation catalyst precursors, we investigated at first their reactivity toward molecular H<sub>2</sub> in model reactions under HPNMR conditions. A solution of Fe(BF<sub>4</sub>)<sub>2</sub>·6H<sub>2</sub>O and *rac*-P4 in PC (1.5 mL, 0.01 M) was initially transferred into a 10 mm medium-pressure HPNMR sapphire tube. <sup>31</sup>P{<sup>1</sup>H} NMR analysis at room temperature under Ar atmosphere showed, as expected, broad signals due to **1**.

Upon addition of CD<sub>3</sub>OD for a deuterium lock (0.5 mL), the <sup>31</sup>P{<sup>1</sup>H} NMR pattern due to **1'** appeared, while no hydride signals were observed in the corresponding <sup>1</sup>H NMR spectrum. The tube was then pressurized at room temperature with 30 bar of H<sub>2</sub>, which resulted in the quantitative conversion of **1** and **1'** into a new species that we identified as **3·BF<sub>4</sub>** on the basis of its <sup>31</sup>P{<sup>1</sup>H} NMR pattern being identical with that of the isolated monohydride **3·BPh<sub>4</sub>**.<sup>21</sup> Due to HPNMR conditions and possible H/D exchange, the Fe–H hydrido ligand appeared as a broad signal centered at ca. –9.16 ppm. In the temperature range 233–353 K, no changes in the spectra were observed, suggesting that a putative hydrido–dihydrogen complex such as [FeH(η<sup>2</sup>-H<sub>2</sub>)(*rac*-P4)]<sup>+</sup> does not form under these conditions, in analogy to what was previously described for [FeH(*meso*-P4)]<sup>+</sup>.<sup>14</sup> This was further verified by repeating the experiment using a 0.025 M solution of **1** in PC/CD<sub>3</sub>OH (3/1, total volume 2.0 mL) and measuring the longitudinal relaxation time (T<sub>1</sub>) at 293 K, respectively, giving values of ca. 900 ms with good exponential fitting of the data, in line with the values expected for a classical hydride.

Complex **2** was remarkably less reactive toward H<sub>2</sub> than **1**. Complex **2** was dissolved in CD<sub>3</sub>OD and reacted with H<sub>2</sub> (30 bar) under HPNMR conditions (see the Supporting Information). At room temperature, in addition to the peaks of unreacted **2**, four distinct <sup>31</sup>P{<sup>1</sup>H} NMR resonances were observed to appear at δ<sub>p</sub> 121.7 (br s), 104.0 (br d), 101.2 (br d), and 96.3 (br s). The corresponding <sup>1</sup>H NMR spectrum showed an apparent doublet of quartets centered at δ<sub>H</sub> –8.5 ppm (dq, <sup>2</sup>J<sub>HPtrans</sub> = 36.7 Hz, <sup>2</sup>J<sub>HPcis,eq</sub> = 51.3 Hz, <sup>2</sup>J<sub>HPcis,ax1</sub> = <sup>2</sup>J<sub>HPcis,ax2</sub> = 51.1 Hz). This pattern, indicative of nonequivalent phosphorus atoms typical of an octahedral Fe complex, was attributed to the formation of *cis-α*-[FeH(NCMe)(*rac*-P4)](BF<sub>4</sub>) (**5**). The resonances due to **3·BF<sub>4</sub>** appeared at 313 K. The temperature was then further increased to 333 and 353 K. The signals due to **3·BF<sub>4</sub>** and **5** were observed to increase, reaching almost complete conversion of **2** with a final 1:3 ratio of ca. 1:3 between **3·BF<sub>4</sub>** and **5**. The reaction is reversible, as cooling to 293 K gave back the same pattern initially observed (Scheme 3 and the Supporting Information). The experiment

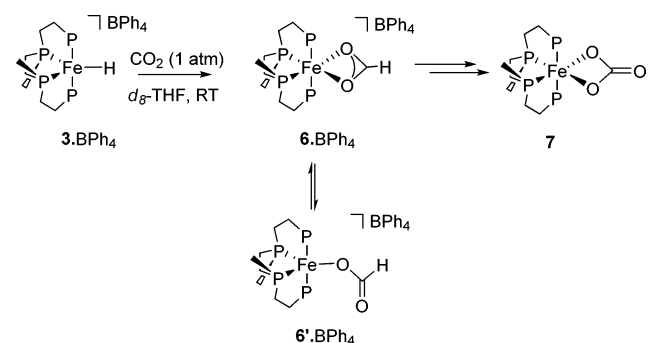
### Scheme 3. Conversion of **2** to **3·BF<sub>4</sub>** and **5**



was repeated in the presence of an added base (NEt<sub>3</sub>), affording at first a mixture of **3·BF<sub>4</sub>** and **5** upon heating, and then **5** as the only product after 20 h of standing at 293 K. Addition of Et<sub>2</sub>O/pentane to the reaction mixture resulted in the precipitation of yellow crystals of **5**. The corresponding X-ray crystal structure, albeit highly disordered, was however useful to confirm the proposed formula (see the Supporting Information).

**Reactivity of 3·BPh<sub>4</sub> and 4 toward CO<sub>2</sub>.** In the next step, we explored the reactivity of the mono- and dihydrides **3·BPh<sub>4</sub>** and **4** toward CO<sub>2</sub>. Beller et al. showed that insertion of CO<sub>2</sub> into the Fe–H bond of the complex [FeH(PP<sub>3</sub>)]<sup>+</sup> could be achieved under 10 atm of gas pressure, giving the corresponding formate complex.<sup>5a</sup> In an NMR-scale experiment, we reacted the monohydride **3·BPh<sub>4</sub>** with CO<sub>2</sub> (1 atm) in *d*<sub>8</sub>-THF, obtaining as expected the formate complex *cis-α*-[Fe(η<sup>2</sup>-O<sub>2</sub>CH)(*rac*-P4)](BPh<sub>4</sub>) (**6·BPh<sub>4</sub>**; Scheme 4), having <sup>31</sup>P{<sup>1</sup>H} NMR signals at δ<sub>p</sub> 106.0 (t) and 76.5 (t, <sup>2</sup>J<sub>PP</sub> = 29.5 Hz). In the corresponding <sup>13</sup>C{<sup>1</sup>H} NMR spectrum, apart from the signal at δ<sub>C</sub> 162.4 ppm due to BPh<sub>4</sub><sup>–</sup>, a broad singlet at 174.6 ppm compatible with a coordinated formate anion was

### Scheme 4. Reactivity of Complex **3·BPh<sub>4</sub>** with H<sub>2</sub> To Give **6·BPh<sub>4</sub>** and **7**



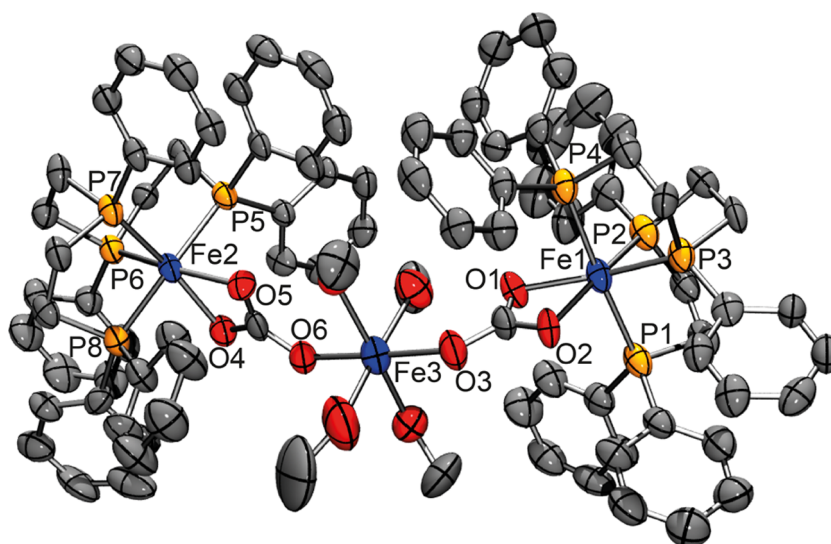


**Figure 4.** Molecular structure for the cationic part of  $\{\mu_2\text{-}[\text{Fe}(\text{MeOH})_4]\text{-}\kappa^1\text{O-}[\text{Fe}(\eta^2\text{-O}_2\text{CO})(\text{rac-P4})]_2\}(\text{BPh}_4)_2$  (**7'**). Ellipsoids are set at the 50% probability level. Hydrogen atoms are omitted for clarity. Selected bond lengths (Å) and bond angles (deg): Fe1–O1, 2.035(5); Fe1–O2, 2.027(5); Fe1–P1, 2.286(3); Fe1–P2, 2.205(3); Fe1–P3, 2.197(2); Fe1–P4, 2.297(3); Fe2–O4, 2.032(5); Fe2–O5, 2.046(5); Fe2–P5, 2.282(2); Fe2–P6, 2.217(3); Fe2–P7, 2.204(2); Fe2–P8, 2.260(2); Fe3–O3, 2.133(6); Fe3–O6, 2.076(6); O1–Fe1–O2, 65.0(2); O1–Fe1–P1, 96.25(17); O1–Fe1–P2, 106.26(19); O1–Fe1–P3, 165.40(18); O1–Fe1–P4, 86.72(17); O2–Fe1–P1, 87.63(17); O2–Fe1–P2, 167.59(17); O2–Fe1–P3, 104.43(18); O2–Fe1–P4, 94.20(17); O4–Fe2–O5, 64.8(2); O4–Fe2–P5, 93.80(16); O4–Fe2–P6, 104.65(17); O4–Fe2–P7, 166.98(19); O4–Fe2–P8, 86.48(16); O5–Fe2–P5, 85.36(16); O5–Fe2–P6, 164.85(16); O5–Fe2–P7, 107.37(16); O5–Fe2–P8, 92.69(17); O3–Fe3–O6, 178.2(2).

**Table 1. Hydrogenation of Sodium Bicarbonate using either in Situ Formed or Defined Molecular Fe(II) Precatalysts<sup>a</sup>**

entry	catalyst precursor	substrate:catalyst	T (°C)	p(H <sub>2</sub> ) (bar)	TON <sup>i,k</sup>	yield (%) <sup>j,k</sup>
1 <sup>b</sup>	i	1000	80	60	154 (±4)	15 (±0)
2 <sup>c</sup>	1''	1000	80	60	62 (±16)	6 (±2)
3 <sup>d</sup>	1	1000	80	60	575 (±52)	58 (±5)
4 <sup>d</sup>	1	1000	100	60	588 (±74)	59 (±7)
5 <sup>d</sup>	1	1000	60	60	186 (±14)	19 (±1)
6 <sup>d</sup>	1	1000	80	30	620 (±36)	62 (±4)
7 <sup>d</sup>	1	1000	80	10	398 (±14)	40 (±1)
8 <sup>e</sup>	1	10000	80	60	83 (±27)	1 (±0)
9 <sup>d,f</sup>	1	3000	80	60	723 (±40)	24 (±1)
10 <sup>g</sup>	2	1000	80	60	762 (±105)	76 (±11)
11 <sup>g</sup>	2	1000	100	60	555 (±15)	55 (±1)
12 <sup>g</sup>	2	1000	60	60	161 (±6)	16 (±1)
13 <sup>g</sup>	2	1000	80	30	766 (±81)	71 (±14)
14 <sup>h</sup>	2	10000	80	60	1229 (±18)	12 (±0)

<sup>a</sup>General reaction conditions: catalyst precursor (0.01 mmol); NaHCO<sub>3</sub> (10 mmol); MeOH (20 mL); H<sub>2</sub> pressure; 24 h. <sup>b</sup>Catalyst precursor i: 1 mL of a 0.01 M stock solution of commercial P4 and Fe(BF<sub>4</sub>)<sub>2</sub>·6H<sub>2</sub>O (1:1). <sup>c</sup>Catalyst precursor 1'': 1 mL of a 0.01 M stock solution of 1'' in PC. <sup>d</sup>Catalyst precursor 1: 1 mL of a 0.01 M stock solution of 1 in PC. <sup>e</sup>0.1 mL of a 0.01 M stock solution of 1 in PC. <sup>f</sup>30.0 mmol of NaHCO<sub>3</sub>. <sup>g</sup>Complex 2 (0.01 mmol) was added to the autoclave from a CH<sub>3</sub>CN stock solution, from which the solvent was subsequently removed (0.02 M, 0.5 mL, see the Experimental Section for details). <sup>h</sup>Complex 2 (0.001 mmol) was added to the autoclave from a CH<sub>3</sub>CN stock solution, from which the solvent was subsequently removed (0.02 M, 50 μL). <sup>i</sup>TON = (mmol of sodium formate)/(mmol of catalyst). <sup>j</sup>Yields calculated from the integration of <sup>1</sup>H NMR signals due to NaHCO<sub>2</sub>, using THF as internal standard. <sup>k</sup>Values of yields and TONs were calculated as averages from the analysis of two to four samples. The largest deviations are reported in parentheses; selected experiments were repeated to ensure reproducibility.

288 observed. By repetition of the test using in situ generated 3-BF<sub>4</sub>  
289 and <sup>13</sup>CO<sub>2</sub>, the singlet at 174.6 ppm turned as expected into a  
290 doublet with <sup>1</sup>J<sub>CH</sub> = 208.8 Hz in the corresponding proton-  
291 coupled <sup>13</sup>C NMR spectrum.<sup>5a,22</sup> Unfortunately, the <sup>1</sup>H NMR  
292 signal expected in the range 8.2–8.5 ppm for the formate  
293 ligand, diagnostic for η<sup>1</sup> vs η<sup>2</sup> coordination, was lying under the  
294 ligand aromatic proton multiplet. After 24 h, the <sup>31</sup>P{<sup>1</sup>H} NMR  
295 spectrum showed signals of a new complex with triplets at δ<sub>p</sub>  
296 106.6 and 73.2 ppm (<sup>2</sup>J<sub>PP</sub> = 30.4 Hz), which we assigned to the  
297 neutral carbonate complex *cis-α*-[Fe(η<sup>2</sup>-O<sub>2</sub>CO)(*rac*-P4)] (**7**).

The corresponding <sup>13</sup>C{<sup>1</sup>H} NMR signal was determined from 298  
the experiment run using <sup>13</sup>CO<sub>2</sub>, giving a singlet at 158.1 ppm. 299  
The attribution was confirmed by independent synthesis of **7** 300  
by reaction of **1** with an excess of K<sub>2</sub>CO<sub>3</sub> in PC. In addition, the 301  
formation of complex **7** was observed also in HPNMR 302  
experiments upon reacting **2** with NaHCO<sub>3</sub> (vide infra). 303  
MeOH diffusion into the d<sub>8</sub>-THF solution recovered after 304  
the NMR experiment described above afforded a few purple 305  
crystals which were found to be suitable for X-ray diffraction 306  
data collection. Quite surprisingly, the solid-state structure 307

308 revealed a trimetallic unit in which a central  $[\text{Fe}(\text{MeOH})_4]^{2+}$   
309 moiety bridges two  $[\text{Fe}(\text{O}_2\text{CO})(\text{rac-P4})]$  moieties via the two  
310 carbonate ligands by  $\eta^1\text{-O}$  coordination, as shown in Figure 4.  
311 Despite the fact that the formation of the complex  $\{\mu_2\text{-}$   
312  $[\text{Fe}(\text{MeOH})_4]\text{-}\kappa^1\text{-O-}[\text{Fe}(\eta^2\text{-O}_2\text{CO})(\text{rac-P4})]_2\}$   $(\text{BPh}_4)_2$  (**7'**)  
313 may be accidental, its solid-state structure confirmed the  
314 presence of  $\text{CO}_3^{2-}$  ligands. Carbonate is likely to form by  
315 reductive disproportionation of  $\text{CO}_2$  into  $\text{CO}_3^{2-}$  and  $\text{CO}$ ,  
316 promoted by  $3\cdot\text{BPh}_4$ .<sup>23</sup> This reaction, occurring via a formate  
317 intermediate, has been previously described with Fe(II) hydrido  
318 complexes such as *trans*- $[\text{Fe}(\text{H})_2(\text{dppe})_2]$  and  $[\text{Fe}$   
319  $(\text{H})_2(\text{PP}_3)]$ .<sup>23,24</sup>

320 Complex **4** was also tested for reactivity with  $\text{CO}_2$ , to check  
321 for the possible formation of Fe hydrido formate complexes,  
322 similarly to what proposed by Beller et al. for  $[\text{Fe}$   
323  $(\text{H})_2(\text{P}^{\text{Ph}}\text{P}_3)]$ .<sup>5f</sup> No reaction was observed under the conditions  
324 described above (i.e., 1 atm of  $\text{CO}_2$  in  $d_8\text{-THF}$ , room  
325 temperature). The experiment was repeated under a moderate  
326 pressure of  $\text{CO}_2$  (7 bar) under HPNMR conditions, but again  
327 no reaction occurred.

### 328 Fe-Catalyzed Sodium Bicarbonate Hydrogenation.

329 The added base-free hydrogenation of sodium bicarbonate to  
330 formate in MeOH was tested in stainless steel autoclaves at  
331 different  $\text{H}_2$  pressures and temperatures. In a preliminary  
332 experiment, we tested the activity of a combination of  
333 commercial tetraphos-1 (**P4**) and  $\text{Fe}(\text{BF}_4)_2\cdot 6\text{H}_2\text{O}$  (0.01  
334 mmol, 1:1 ratio) in the hydrogenation of sodium bicarbonate  
335 in MeOH. To our delight, at 80 °C under 60 bar  $\text{H}_2$ , sodium  
336 formate was formed with TON = 154 (entry 1). The activity of  
337 **1** and **1''** was then tested to check for ligand effects. The *in situ*  
338 formed precatalysts were obtained from stock solutions made  
339 from  $\text{Fe}(\text{BF}_4)_2\cdot 6\text{H}_2\text{O}$  and either *rac*-**P4** or *meso*-**P4** (0.01 M in  
340 PC). The solutions were analyzed by  $^{31}\text{P}\{^1\text{H}\}$  NMR before use  
341 to confirm the formation of the corresponding Fe(II)  
342 complexes **1** and **1''**. Catalyst precursor **1''** gave a rather poor  
343 catalytic performance, reaching a TON value of 62 after 24 h  
344 under 60 bar of  $\text{H}_2$  and 80 °C using 0.1 mol % catalyst (Table  
345 1; entry 2). In contrast, **1** was rather active in the catalytic  
346 hydrogenation of  $\text{NaHCO}_3$  in MeOH. Under 60 bar of  $\text{H}_2$   
347 pressure, using 0.1 mol % of atalyst, rather good yields (58%  
348 and 59%) and TONs (575 and 588) were achieved at 80 and  
349 100 °C, respectively (Table 1; entries 3 and 4). TON values are  
350 on the same order of magnitude as those obtained by Beller et  
351 al. with the  $\text{Fe}(\text{BF}_4)_2/\text{PP}_3$  system under comparable con-  
352 ditions.<sup>5a</sup> At 60 °C (entry 5) the TON decreased to 186 with a  
353 formate yield of 19%. The effect of  $\text{H}_2$  pressure on the  
354 productivity of the reaction was also tested. TON and yield  
355 were not affected at 80 °C in passing from 60 to 30 bar (entry  
356 6), whereas at 10 bar the yield of formate was slightly reduced  
357 (entry 7). Using a catalyst to substrate ratio of 1:10000,  
358 significantly lower TON and yield were obtained (entry 8). At  
359 an intermediate catalyst to substrate ratio (1:3000, obtained by  
360 increasing the substrate concentration) good activity was  
361 observed with TON = 723 and 24% yield in formate (entry  
362 9). The hydrogenation of  $\text{NaHCO}_3$  to  $\text{NaHCO}_2$  using the well-  
363 defined molecular complex **2** as the catalyst precursor (0.1 mol  
364 %) proceeded smoothly at 80 °C, affording sodium formate in  
365 excellent yields (76 and 71%) and good TONs (762 and 766)  
366 under 60 and 30 bar of  $\text{H}_2$  pressure (entries 10 and 13,  
367 respectively). When the catalyst loading was lowered to 0.01  
368 mol %, an increased TON = 1229 was measured, albeit with a  
369 lower yield in formate (12%) (entry 14). At this catalyst to  
370 substrate ratio, **2** performed better than **1** (1.2 mmol of sodium

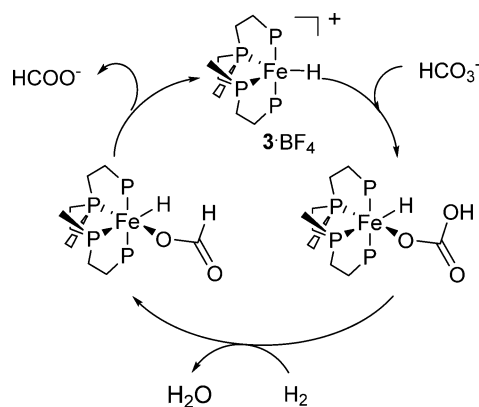
formate vs ca. 0.1 mmol obtained; entries 14 and 8, 371  
372 respectively). Finally, at higher (100 °C) or lower temperatures  
373 (60 °C) in the presence of **2** (0.1 mol %), lower yields of  
374 formate were obtained (entries 11 and 12). On the basis of  
375 these results, we propose that the better performance of the *rac*  
376 vs *meso* systems can be related to the preferred *cis* conformation  
377 of the former, suitable for an inner-sphere mechanism (vide  
378 infra). In the case of *meso*-**P4**, different isomers can form in  
379 solution (Scheme 1), hence decreasing the concentration of the  
380 likely active form, i.e. *cis*-**β**-**2** (Scheme 2).

**Mechanistic Studies.** To gain mechanistic insights into the  
381 iron-catalyzed hydrogenation of  $\text{NaHCO}_3$  to sodium formate in  
382 the presence of **1** and **2**, we monitored catalyst evolution by  
383 HPNMR spectroscopy under *operando* conditions. In detail,  
384 a 10 mm HPNMR sapphire tube was initially charged with a  
385 0.01 M solution of **1** in PC (1.5 mL),  $\text{CD}_3\text{OD}$  (0.5 mL), and  
386  $\text{NaHCO}_3$  (84 mg; 1.0 mmol, 100 equiv). The  $^{31}\text{P}\{^1\text{H}\}$  NMR  
387 pattern showed the presence of **1** (25%), **1'** (25%), and the  
388 new species **8** (50%) (percentages are based on integrals),  
389 characterized by two triplets at  $\delta_{\text{p}}$  107.1 and 72.9 ppm ( $^2J_{\text{PP}} =$   
390 30.3 Hz).<sup>25</sup> Pressurization of the reaction mixture with  $\text{H}_2$  (30  
391 bar) resulted in the formation of the monohydride complex **3**·  
392  $\text{BF}_4$  (34%) at room temperature. The mixture composition  
393 evolved fully to **3**· $\text{BF}_4$  in less than 2 h upon slow heating to 60  
394 °C, as confirmed by  $^{31}\text{P}\{^1\text{H}\}$  NMR spectra. Further heating to  
395 80 °C did not result in further changes of the NMR patterns. A  
396 similar experiment was carried out using **2** (0.01 mmol) and  
397  $\text{NaHCO}_3$  (100 equiv) in  $\text{CD}_3\text{OD}$  (2 mL). The initial mixture  
398 prepared under an Ar atmosphere showed in the corresponding  
399  $^{31}\text{P}\{^1\text{H}\}$  NMR the presence of unreacted **2** (84%), **1'** (7%), and  
400 **7** (9%). Upon standing at room temperature for 75 min, the  
401 resonances observed for **1'** and **7** increased significantly (up to  
402 34% and 27%), by slow reaction of **2** with  $\text{NaHCO}_3$ . The slow  
403 ligand exchange from  $\text{CH}_3\text{CN}$  to  $\text{CO}_3^{2-}$  mirrors the reactivity  
404 of **2** with  $\text{H}_2$  described above. By pressurization of the HPNMR  
405 tube with  $\text{H}_2$  (30 bar), the resonances due to **5** appeared in the  
406  $^{31}\text{P}\{^1\text{H}\}$  and  $^1\text{H}$  NMR spectra, already at room temperature. At  
407 80 °C, the signals of **2**, **1'**, and **7** disappeared, with concomitant  
408 formation of **3**· $\text{BF}_4$  and **5** and free sodium formate (broad  
409 signals at 8.6–8.9 ppm in the  $^1\text{H}$  NMR spectrum).<sup>26</sup>

The experimental results clearly indicate in **3**· $\text{BF}_4$  the key  
411 intermediate in the catalytic hydrogenation of  $\text{NaHCO}_3$  with **1**  
412 and **2**, similarly to what was described by Beller and co-workers  
413 in the case of  $\text{CO}_2$  hydrogenation by  $[\text{Fe}(\text{H})(\text{PP}_3)]^+$ .<sup>5a</sup> Despite  
414 the fact that we could not observe other catalytic intermediates  
415 in addition to **3** under HPNMR conditions, an outer-sphere  
416 mechanism involving intermolecular hydride transfer is  
417 unlikely, as it would not account for the different catalytic  
418 activities observed for *rac* and *meso* systems. In contrast, we  
419 suggest that an inner-sphere mechanism requiring two available  
420 *cis* positions would be more likely and consistent with the  
421 better catalytic activity observed using **1**. A proposed  
422 mechanism for  $\text{NaHCO}_3$  hydrogenation centered on **3** is  
423 shown in Scheme 5.

**Formic Acid Dehydrogenation.** FA dehydrogenation to  
425  $\text{H}_2/\text{CO}_2$  gas mixtures was tested in the presence of the *in situ*  
426 and preformed catalysts described above, using an inert solvent  
427 (PC) under isobaric conditions (1 atm) and in the absence of  
428 added base, the development of gas during the reaction being  
429 measured with a manual gas buret. The gas mixtures were  
430 analyzed off-line by FT-IR spectroscopy, showing the absence  
431 of CO for all tests (detection limit 0.02%).<sup>27</sup> Much to our  
432 surprise, the well-defined catalyst precursor **2** (0.1 mol %) was  
433

### Scheme 5. Proposed Mechanism for the Catalytic Hydrogenation of NaHCO<sub>3</sub> in the Presence of 3



inactive in the dehydrogenation of FA in PC at 40 °C. Thus, we targeted the use of in situ catalysts formed using *rac*- and *meso*-P4. Initially, we checked the activity of commercial P4 (0.01 mol %, *meso/rac* = ca. 3) under the same conditions described above and observed a FA conversion of 4% after 6 h, corresponding to TON = 444 (Table 2; entry 1). When pure *rac*-P4 was used, generating in situ catalyst 1 (0.1 mol %), FA dehydrogenation proceeded with good conversions, reaching TON = 604 after 8 h at 40 °C (entry 2). As reported for the PP<sub>3</sub>/Fe(BF<sub>4</sub>)<sub>2</sub>·6H<sub>2</sub>O catalyst system,<sup>5c</sup> higher ligand/Fe ratios are beneficial to reach high reaction turnovers. Using a Fe/*rac*-P4 = 1/2 ratio,<sup>5c</sup> as expected the catalyst performance improved significantly, affording full conversion of FA in ca. 6 h (TON = 1000; entry 3). Using a catalyst to substrate ratio of 1:10000 at 40 °C, low conversions (11%) were obtained after 6 h, with TON = 1081 (entry 5). Using the same catalyst to substrate ratio at 60 °C gave a higher TON value of 3088 after 6 h (entry 6). Using a higher Fe to ligand ratio (1:4) at 60 °C, considerably enhanced catalytic activity was achieved (TON = 6061, 6 h; entry 9). In contrast, precatalysts obtained from Fe(BF<sub>4</sub>)<sub>2</sub>·6H<sub>2</sub>O and *meso*-P4 showed worse catalytic activities (generally ca. 33% lower) in comparison to *rac*-P4 (entries 4, 7, 8, and 10). Also in this case, the exclusive *cis* geometry forced by *rac*-P4 is the most suitable to convey a catalytically active species, in comparison to *meso*-P4, for which different geometrical isomers are possible. Selected results are summarized in Table 2. Selected reaction profiles (volumes

vs time) of catalytic runs obtained at a catalyst to substrate ratio of 1:10000, at various Fe to ligand ratios and temperatures, are shown in Figure 5. Disappointingly, recycling experiments with catalyst:substrate = 1:1000, Fe:ligand = 1:2, and 40 °C showed a severe drop in activity from the first to the third cycle, namely from TON = 1000 to 295 after 6 h.

**Mechanistic Studies.** The reactivity of the different precatalysts with FA was studied by monitoring stoichiometric reactions with NMR and by HPNMR under in operando conditions. A solution of complex 2 (0.7 mL, 0.012 M in PC, C<sub>6</sub>D<sub>6</sub> insert) was reacted with FA (1 equiv) for 1 h in a NMR tube. No changes in the <sup>31</sup>P{<sup>1</sup>H} and <sup>1</sup>H NMR spectra were observed even after heating to 60 °C, confirming that 2 is not reactive under these conditions, probably due to stable coordination of MeCN ligands to the Fe center.

In contrast, addition of 1 equiv of FA to a solution of 1 in PC in a NMR tube (0.7 mL, 0.042 M, C<sub>6</sub>D<sub>6</sub> insert) at room temperature resulted in the formation of the monohydride [FeH(*rac*-P4)](BF<sub>4</sub>) (3-BF<sub>4</sub>) and of the formate complex [Fe(η<sup>2</sup>-O<sub>2</sub>CH)(*rac*-P4)](BF<sub>4</sub>) (6-BF<sub>4</sub>), initially in a 6:1 ratio. Heating to 40 °C for 1 h and then leaving the tube overnight at 25 °C gave almost complete conversion to 3-BF<sub>4</sub>. The experiment was repeated in the presence of a large excess of FA (100 equiv), with catalyst evolution monitored by HPNMR spectroscopy. A 10 mm HPNMR sapphire tube was thus charged with a solution of 1 in PC (1.8 mL; 0.012 M), to which CD<sub>3</sub>OD (0.4 mL) was added for deuterium lock. Upon addition of FA at room temperature, complexes 3-BF<sub>4</sub> and 6-BF<sub>4</sub> were observed to form in a 1:6 ratio. The probe head was then heated to 40 °C. After 1 h, the reaction mixture evolved further with formation of a new species (9), characterized by four structured signals in the <sup>31</sup>P{<sup>1</sup>H} NMR (see the Experimental Section) and by a complex high-field resonance signal (ddd; δ<sub>H</sub> -9.55 ppm, <sup>2</sup>J<sub>PP</sub> = 25.5, 46.5, 70.7 Hz; 1H, FeH) in the corresponding <sup>1</sup>H NMR spectrum, indicative of the formation of an octahedral [FeHL(*rac*-P4)] complex with *cis*-α configuration. Prolonged heating resulted in complete conversion to 9, affording a yellow solution. Further multinuclear NMR analysis and ESI-MS spectroscopy data obtained from aliquots of the final solution allowed us to identify complex 9 as the Fe carbonyl hydrido complex *cis*-α-[FeH(CO)(*rac*-P4)](BF<sub>4</sub>) (L = CO; for details see the Experimental Section).

**Table 2. Formic Acid Dehydrogenation Catalyzed using in Situ Fe(II) Precatalysts**

entry	ligand	substrate:catalyst	Fe/ligand	T (°C)	V <sub>1h</sub> (mL) <sup>d</sup>	TON <sub>1h</sub> <sup>e</sup>	TOF <sub>10min</sub> <sup>f</sup>	V <sub>final</sub> (mL) <sup>d</sup>	TON <sub>final</sub> <sup>e</sup>	total conversn (%)
1 <sup>a</sup>	P4 <sup>c</sup>	10000	1:2	40	25	97	232	115	444 (6 h)	4
2 <sup>a</sup>	<i>rac</i> -P4	1000	1:1	40	220	85	35	1560	604 (8 h)	60
3 <sup>a</sup>	<i>rac</i> -P4	1000	1:2	40	345	133	139	2570	1000 (6 h)	100
4 <sup>a</sup>	<i>meso</i> -P4	1000	1:2	40	165	64	151	810	313 (8 h)	31
5 <sup>b</sup>	<i>rac</i> -P4	10000	1:2	40	45	174	347	280	1081 (6 h)	11
6 <sup>b</sup>	<i>rac</i> -P4	10000	1:2	60	215	830	1853	800	3088 (6 h)	31
7 <sup>b</sup>	<i>meso</i> -P4	10000	1:2	40	15	58	116	90	348 (6 h)	3
8 <sup>b</sup>	<i>meso</i> -P4	10000	1:2	60	70	270	579	260	1003 (6 h)	10
9 <sup>b</sup>	<i>rac</i> -P4	10000	1:4	60	400	1544	1737	1570	6061 (6 h)	61
10 <sup>b</sup>	<i>meso</i> -P4	10000	1:4	60	140	540	579	590	2278 (8 h)	23

<sup>a</sup>Reaction conditions: Fe(BF<sub>4</sub>)<sub>2</sub>·6H<sub>2</sub>O, 5.3 mmol; ligand, 1–4 equiv with respect to Fe; HCOOH, 5.3 mol (2 mL); PC, 5 mL. <sup>b</sup>Reaction conditions as in footnote a, except for the following: Fe(BF<sub>4</sub>)<sub>2</sub>·6H<sub>2</sub>O, 5.3 μmol. <sup>c</sup>Commercial tetraphos-1 (P4) ligand, *meso*-P4:*rac*-P4 = 3. <sup>d</sup>Gas evolution measured by manual gas buret, based on two to four tests, error ±10%. (Gas mixture analyzed off-line by FTIR spectroscopy. <sup>e</sup>Defined as (mmol of gas produced)/(mmol of catalyst). <sup>f</sup>Defined as (mmol of gas produced)/(mmol of catalyst) h, calculated at conversions observed after 10 min.

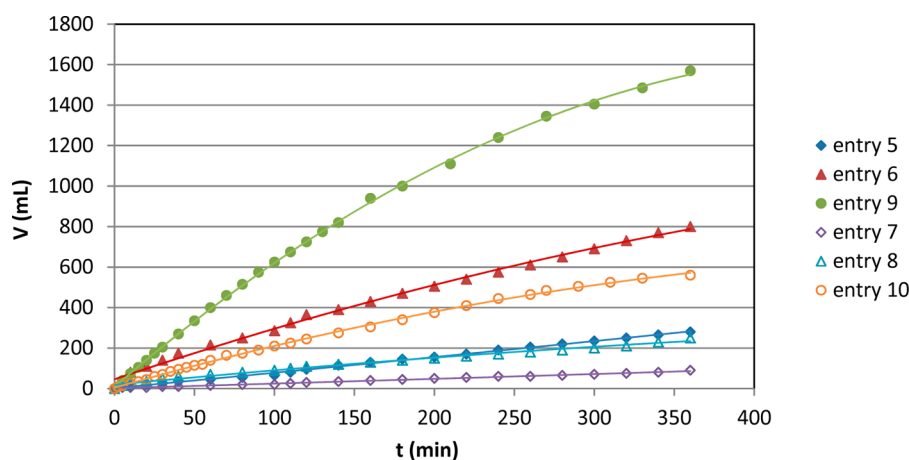


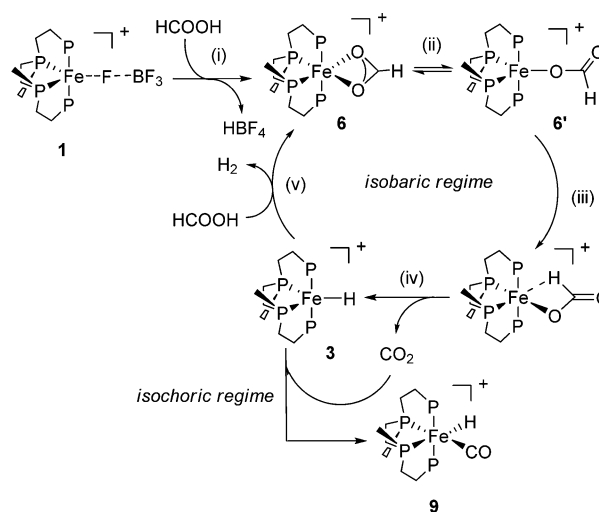
**Figure 5.** Reaction profiles of selected FA dehydrogenation catalytic runs using a catalyst to substrate ratio of 1:10000 at different temperatures and Fe:P4 ratios. For legends and conditions, see Table 2.

As CO may result from a competitive FA decomposition pathway, i.e. dehydration to H<sub>2</sub>O and CO, we thought it was of interest to investigate further the reaction of **1** with FA. Some hints were given from the experimental data described above. First, CO was never detected in the gas mixtures resulting from the catalytic runs by off-line FTIR measurements (see the Supporting Information for a representative spectrum).<sup>27</sup> Second, complex **9** was never obtained in the NMR experiment carried out using an FA to **1** ratio of 1:1. Third, **9** was formed under isochoric conditions (HPNMR) in the presence of 100 equiv of FA. Under these conditions, it is likely that the CO<sub>2</sub> pressure built up in the HPNMR tube during the course of the experiment may have undergone partial reductive disproportionation to CO and CO<sub>3</sub><sup>2-</sup>, as previously observed upon prolonged reaction of the monohydride **3**·BPh<sub>4</sub> with CO<sub>2</sub>.

To confirm this hypothesis, we repeated the experiment in the glass reactor (isobaric conditions) normally used for the catalytic runs. Under the same conditions applied for the HPNMR experiment, gas evolution was complete after 20 min and again no CO was detected in the gas mixture. Furthermore, the mixture remained purple throughout the run, whereas a bright yellow should be expected upon formation of **9** in high concentrations. As further confirmation, NMR analysis of the catalytic mixture at the end of the run showed the typical <sup>31</sup>P{<sup>1</sup>H} NMR resonances of **3**·BF<sub>4</sub> and **6**·BF<sub>4</sub> in a 1:1 ratio, while signals due to **9** were not observed. On the basis of these data, although we cannot rule out that at low catalyst concentrations (0.01 mol %) catalyst deactivation may occur by formation of **9**, we propose that in closed (isochoric) vessels Fe-catalyzed CO<sub>2</sub> reductive disproportionation becomes a competing pathway, and CO coordination to **3**·BF<sub>4</sub> gives the stable (and catalytically inactive) octahedral **9**.

The pathway for the base-free FA catalytic dehydrogenation reaction is thus proposed as shown in Scheme 6. In step (i), the catalyst precursor **1**, formed in situ from Fe(BF<sub>4</sub>)<sub>2</sub>·6H<sub>2</sub>O and *rac*-P4, reacts with FA to give the formate complex [Fe(η<sup>2</sup>-O<sub>2</sub>CH)(*rac*-P4)](BF<sub>4</sub>) (**6**·BF<sub>4</sub>), which after a η<sup>2</sup> → η<sup>1</sup> coordination shift from **6** to **6'** (ii) and rearrangement (iii) undergoes β-hydride elimination to give back **3**·BF<sub>4</sub> and CO<sub>2</sub> (iv). Protonation of **3**·BF<sub>4</sub> by FA results in the fast elimination of H<sub>2</sub> and regeneration of the formate complex **6**·BF<sub>4</sub> (v).

### Scheme 6. Proposed Mechanism for the Catalytic Dehydrogenation of FA



## CONCLUSIONS

In summary, the coordination chemistry of the *rac* and *meso* isomers of the linear tetraphosphine 1,1,4,7,10,10-hexaphenyl-1,4,7,10-tetraphosphadecane (tetraphos-1, P4) toward Fe(II) was explored in detail, giving novel complexes which were applied as catalysts for base-free H<sub>2</sub>/CO<sub>2</sub> generation from formic acid and for the hydrogenation of sodium bicarbonate to formate under mild conditions, showing a higher activity in the case of Fe/*rac*-P4 systems. Mechanistic studies highlighted the pivotal role of the monohydride [FeH(*rac*-P4)]<sup>+</sup> in both reactions and showed that CO<sub>2</sub> reductive disproportionation should not be underestimated as a competing pathway in the case of Fe(II)/polyphosphine systems. A full DFT study of both catalytic reactions promoted by Fe/tetraphos-1 is currently under way.

## EXPERIMENTAL SECTION

**General Methods and Materials.** All syntheses were performed using standard Schlenk techniques under an atmosphere of dry nitrogen or argon. Solvents were freshly distilled over appropriate drying agents, collected over Linde type 3A or 4A molecular sieves under nitrogen, and degassed with nitrogen or argon gas. The ligand 1,1,4,7,10,10-



567 hexaphenyl-1,4,7,10-tetraphosphadecane (tetraphos-1, P4) was  
568 supplied by Pressure Chemicals Inc., Pittsburgh, PA.  $^{13}\text{C}$ -  
569 labeled carbon dioxide (99 atom %  $^{13}\text{C}$ ) was purchased from  
570 Sigma-Aldrich.  $[\text{Fe}(\text{MeCN})_6](\text{BF}_4)_2$  was synthesized according  
571 to literature methods.<sup>17</sup> Anhydrous  $\text{FeCl}_2$ ,  $\text{Fe}(\text{BF}_4)_2 \cdot 6\text{H}_2\text{O}$ , and  
572 propylene carbonate (PC) were purchased from commercial  
573 suppliers and used without further purification.

574 **Synthetic Procedures. Reaction of *rac*-P4 with  $\text{Fe}(\text{BF}_4)_2 \cdot$   
575  $6\text{H}_2\text{O}$ .** The ligand *rac*-P4 (67 mg, 0.1 mmol) was dissolved in  
576 propylene carbonate (PC; 2.0 mL) with gentle heating (40–50  
577 °C) to afford complete dissolution. One equivalent of  
578  $\text{Fe}(\text{BF}_4)_2 \cdot 6\text{H}_2\text{O}$  (34 mg, 0.1 mmol) was added to the colorless  
579 solution, which immediately turned deep purple.  $^{31}\text{P}\{^1\text{H}\}$  NMR  
580 analysis showed quantitative formation of a single product. The  
581 purple product could be precipitated by adding a large amount  
582 of  $\text{Et}_2\text{O}$  (at least 8.0 mL). The decanted solid was recovered by  
583 removing the colorless solution via cannula and washed with  
584  $\text{Et}_2\text{O}$  to remove all propylene carbonate, yielding the  
585 analytically pure complex  $[\text{Fe}(\eta^1\text{-FBF}_3)(\text{rac-P4})](\text{BF}_4)$  (**1**).  
586 Due to the poor stability of **1** as an isolated solid, we chose to  
587 use stock solutions of **1** in PC for both catalytic and NMR  
588 experiments. Yield: 78 mg (94%).  $^{31}\text{P}\{^1\text{H}\}$  NMR (121.49 MHz,  
589 PC +  $\text{C}_6\text{D}_6$  capillary):  $\delta_{\text{p}}$  99.8 (br s; 2P, PPh), 60.9 ppm (br s;  
590 2P, PPh<sub>2</sub>).  $^{19}\text{F}\{^1\text{H}\}$  NMR (376.15 MHz, PC +  $\text{C}_6\text{D}_6$  insert):  $\delta_{\text{p}}$   
591 154 ppm (s; 4F,  $\text{BF}_4$ ).

592 **Reaction of *meso*-P4 with  $\text{Fe}(\text{BF}_4)_2 \cdot 6\text{H}_2\text{O}$ .** In a 5 mm NMR  
593 tube, *rac*-P4 (20 mg, 0.03 mmol) was dissolved in propylene  
594 carbonate (PC; 0.7 mL). Gentle heating (40–50 °C) was  
595 needed to afford complete dissolution of the ligand. One  
596 equivalent of  $\text{Fe}(\text{BF}_4)_2 \cdot 6\text{H}_2\text{O}$  (10 mg, 0.03 mmol) was added  
597 to the colorless solution, which immediately turned brown and  
598 then yellow.  $^{31}\text{P}\{^1\text{H}\}$  NMR analysis showed the formation of  
599  $[\text{Fe}(\eta^1\text{-FBF}_3)(\text{meso-P4})](\text{BF}_4)$  (**1''**) as a single product. No  
600 attempts were made to isolate the product.  $^{31}\text{P}\{^1\text{H}\}$  NMR  
601 (121.49 MHz, PC +  $\text{C}_6\text{D}_6$  insert):  $\delta_{\text{p}}$  104.2 (br s; 2P, PPh),  
602 70.5 ppm (br s; 2P, PPh<sub>2</sub>).

603 **Synthesis of *cis*- $\alpha$ - $[\text{Fe}(\text{MeCN})_2(\text{rac-P4})](\text{BF}_4)_2$  (**2**).** The ligand  
604 *rac*-P4 (134 mg, 0.2 mmol) was suspended in MeCN (10.0  
605 mL), and the mixture was vigorously stirred until the  
606 tetraphosphine turned into a thin powder. One equivalent of  
607  $[\text{Fe}(\text{MeCN})_6](\text{BF}_4)_2$  (95 mg, 0.2 mmol) was added to the  
608 white suspension, affording a bright orange solution. The  
609 reaction mixture was stirred until a clear solution was obtained  
610 and was subsequently stirred 1 h more. The solution was then  
611 concentrated under vacuum to remove all volatiles. The  
612 resulting orange solid was then dissolved in a minimum  
613 volume of acetonitrile (ca. 0.5 mL). Addition of pentane  
614 resulted in the precipitation of analytically pure **2** as a  
615 crystalline, orange solid. Yield: 170 mg (87%). Crystals of **2**  
616 suitable for X-ray diffraction data collection were grown by  
617 adding pentane (4.0 mL) to an acetonitrile/methanol solution  
618 (0.5 + 1.0 mL) of **2**.  $^{31}\text{P}\{^1\text{H}\}$  NMR (121.49 MHz,  $\text{CD}_3\text{CN}$ ):  $\delta_{\text{p}}$   
619 100.7 (t,  $^2J_{\text{PP}} = 31.7$  Hz; 2P, PPh), 65.6 ppm (t,  $^2J_{\text{PP}} = 31.7$  Hz;  
620 2P, PPh<sub>2</sub>). ESI-MS: calcd for  $^{12}\text{C}_{46}^{1}\text{H}_{48}^{14}\text{N}_2^{56}\text{Fe}^{31}\text{P}_4$  ( $[\text{M}]^+$ )  $m/z$   
621  $z$  404.10532, found  $m/z$  404.10474.

622 **Reaction of *meso*-P4 with  $[\text{Fe}(\text{MeCN})_6](\text{BF}_4)_2$ .** In an NMR-  
623 scale experiment, *meso*-P4 (13 mg, 0.02 mmol) was placed into  
624 an NMR tube, to which 0.5 mL of  $\text{CD}_3\text{CN}$  was added. The  
625 NMR tube was shaken vigorously to help dissolution of the  
626 ligand, and subsequently  $[\text{Fe}(\text{MeCN})_6](\text{BF}_4)_2$  (ca. 10 mg, 0.02  
627 mmol) was added, resulting in an immediate color change to  
628 red-orange. The reaction mixture was analyzed by  $^{31}\text{P}\{^1\text{H}\}$   
629 NMR, which showed the formation of *trans*- $[\text{Fe}$

$(\text{MeCN})_2(\text{meso-P4})](\text{BF}_4)_2$  (*trans*-**2**) and *cis*- $\beta$ - $[\text{Fe}$  630  
 $(\text{MeCN})_2(\text{meso-P4})](\text{BF}_4)_2$  (*cis*- $\beta$ -**2**) in an approximately 2:1 631  
ratio.  $^{31}\text{P}\{^1\text{H}\}$  NMR for *trans*-**2** (121.49 MHz,  $\text{CD}_3\text{CN}$ ):  $\delta_{\text{p}}$  632  
85.4 (m; 2P, PPh), 75.4 (m; 2P, PPh<sub>2</sub>).  $^{31}\text{P}\{^1\text{H}\}$  NMR for *cis*- $\beta$ - 633  
**2** (121.49 MHz,  $\text{CD}_3\text{CN}$ ):  $\delta_{\text{p}}$  115.2 (m; 1P), 111.4 (m; 1P), 634  
72.1 (m; 1P), 59.9 (m; 1P). 635

**Synthesis of  $[\text{FeH}(\text{rac-P4})](\text{BPh}_4)$  (**3-BPh**<sub>4</sub>).** In a flame-dried 636  
Schlenk tube kept under argon, *rac*-P4 (67 mg, 0.1 mmol) was 637  
dissolved in 3.0 mL of THF. A stoichiometric amount of 638  
anhydrous  $\text{FeCl}_2$  (13 mg, 0.1 mmol) was added as a solid, and 639  
the resulting deep blue solution was stirred for 5 min at room 640  
temperature.  $\text{NaBPh}_4$  (35 mg; 0.01 mmol) and MeOH (1.5 641  
mL) were added to the reaction mixture, which was then stirred 642  
vigorously for about 10 min.  $\text{NaBH}_4$  (4 mg, 0.1 mmol) was 643  
then added to the reaction mixture as a solid, and a vigorous 644  
reaction took place, affording an intense red mixture. All 645  
volatiles were removed under vacuum, and the solid residue was 646  
redissolved in THF (8.0 mL). The resulting suspension was 647  
filtered via cannula into a second Schlenk tube kept under 648  
argon, affording a limpid red solution, from which all volatiles 649  
were removed under vacuum, affording NMR-pure **3-BPh**<sub>4</sub>. 650  
Yield: 103 mg (95%). Crystals suitable for X-ray diffraction data 651  
collection were obtained by adding MeOH to a THF solution 652  
of **3-BPh**<sub>4</sub>.  $^{31}\text{P}\{^1\text{H}\}$  NMR ( $d_8$ -THF, 121.49 MHz):  $\delta_{\text{p}}$  119.4 (t, 653  
 $^2J_{\text{PP}} = 24.5$  Hz; 2P, PPh), 99.4 (t,  $^2J_{\text{PP}} = 24.5$  Hz; 2P, PPh<sub>2</sub>).  $^1\text{H}$  654  
NMR ( $d_8$ -THF, 300.13 MHz, negative region):  $\delta_{\text{H}}$  -9.16 (t, 655  
 $^2J_{\text{HP}} = 24.0$  Hz; 1H, FeH). 656

**Synthesis of *cis*- $\alpha$ - $[\text{Fe}(\text{H})_2(\text{rac-P4})]$  (**4**).** The synthetic 657  
procedure described for the synthesis of *trans*- $[\text{Fe}(\text{H})_2(\text{meso-}$  658  
 $\text{P4})]$  was adapted with slight modifications.<sup>14</sup> A three-necked 659  
round-bottom flask equipped with a reflux condenser was 660  
charged under argon with *rac*-P4 (67 mg, 0.1 mmol) and dry 661  
THF (2.5 mL). A solution of anhydrous  $\text{FeCl}_2$  (13 mg, 0.1 662  
mmol) in THF (2.5 mL) was added via cannula, and the 663  
resulting mixture was stirred for 10 min.  $\text{NaBH}_4$  (20 mg, 0.55 664  
mmol) was added as a solid, and the dark blue reaction mixture 665  
that was obtained was heated to reflux. As no visible changes 666  
occurred, additional THF (3.0 mL) was added, followed by 667  
another aliquot of  $\text{NaBH}_4$  (10 mg, 0.27 mmol) and absolute 668  
EtOH (0.5 mL). As EtOH was added, a vigorous reaction took 669  
place and the deep blue mixture turned orange. After gas 670  
evolution had ceased, additional  $\text{NaBH}_4$  (10 mg, 0.27 mmol) 671  
and absolute EtOH (0.5 mL) were added, and again, gas 672  
evolution was observed. The orange mixture was refluxed for 673  
about 10 min after gas evolution had ceased, after which it was 674  
cooled to room temperature and filtered via cannula. The 675  
volume of the solution was partially reduced under vacuum, and 676  
dry methanol was subsequently layered on top of the orange 677  
solution, from which bright yellow crystals formed. Yield: 53 678  
mg (72%).  $^{31}\text{P}\{^1\text{H}\}$  NMR ( $d_8$ -THF, 121.49 MHz):  $\delta_{\text{p}}$  123.8 (t, 679  
 $^2J_{\text{PP}} = 13.5$  Hz; 2P, PPh), 113.1 (t,  $^2J_{\text{PP}} = 13.5$ ; 2P, PPh<sub>2</sub>).  $^1\text{H}$  680  
NMR ( $d_8$ -THF, 300.13 MHz, negative region):  $\delta_{\text{H}}$  -11.7 (m; 681  
2H,  $\text{Fe}(\text{H})_2$ ). ESI-MS: calcd for  $^{12}\text{C}_{42}^{1}\text{H}_{43}^{56}\text{Fe}^{31}\text{P}_4$  ( $[\text{M} - \text{H}]^+$ ) 682  
 $m/z$  727.16592, found  $m/z$  727.16523. 683

**Reaction of **3-BPh**<sub>4</sub> with  $\text{CO}_2$ .** A few crystals of **3-BPh**<sub>4</sub> (ca. 684  
10 mg) were placed in an NMR tube under argon and dissolved 685  
in  $d_8$ -THF (0.5 mL).  $\text{CO}_2$  (1 atm) was then bubbled through 686  
the solution, which then turned light purple. NMR analysis 687  
revealed quantitative formation of the expected formate 688  
complex  $[\text{Fe}(\eta^1\text{-OCHO})(\text{rac-P4})](\text{BPh}_4)$  (**6-BPh**<sub>4</sub>).  $^{31}\text{P}\{^1\text{H}\}$  689  
NMR for **6-BPh**<sub>4</sub> ( $d_8$ -THF, 161.99 MHz):  $\delta_{\text{p}}$  106.0 (t,  $^2J_{\text{PP}} =$  690  
28.5 Hz; 2P, PPh), 76.5 (t,  $^2J_{\text{PP}} = 26.1$  Hz; 2P, PPh<sub>2</sub>).  $^{13}\text{C}\{^1\text{H}\}$  691

692 NMR for **6**-BPh<sub>4</sub> (*d*<sub>8</sub>-THF, 100.6 MHz):  $\delta_C$  162.4 (dd;  $^2J_{PP} =$   
693 49.4 Hz,  $^2J_{PP} = 98.7$  Hz, BPh<sub>4</sub>), 174.6 (br s, Fe(O<sub>2</sub>CH)).

694 After 24 h acquisition, the  $^{31}\text{P}\{^1\text{H}\}$  NMR spectrum revealed  
695 the formation of the carbonate complex [Fe( $\eta^2$ -O<sub>2</sub>CO)(*rac*-  
696 P4)] (**7**). On the basis of  $^{31}\text{P}\{^1\text{H}\}$  NMR integration, complexes  
697 **6** and **7** resulted in an approximately 1:0.6 ratio.  $^{31}\text{P}\{^1\text{H}\}$  NMR  
698 for **7** (*d*<sub>8</sub>-THF, 161.99 MHz):  $\delta_P$  106.6 (t,  $^2J_{PP} = 30.4$  Hz; 2P,  
699 PPh), 73.2 (t,  $^2J_{PP} = 30.4$  Hz; 2P, PPh<sub>2</sub>). No  $^{13}\text{C}\{^1\text{H}\}$  NMR  
700 resonance was observed for the carbonate O<sub>2</sub>CO carbon atom  
701 of **7**. The experiment was repeated using 3-BF<sub>4</sub> and  $^{13}\text{CO}_2$ ,  
702 showing the same  $^{31}\text{P}\{^1\text{H}\}$  NMR and  $^{13}\text{C}$  NMR (proton  
703 coupled) signals at 174.6 (d,  $^1J_{CH} = 208.8$  Hz) and 158.1 ppm  
704 (s) for **6** and **7**, respectively.

705 A few purple crystals suitable for X-ray diffraction data  
706 collection were obtained by layering MeOH on top of the *d*<sub>8</sub>-  
707 THF solution and standing for 1 day. The X-ray crystal  
708 structure revealed the serendipitous formation of the trimetallic  
709 complex  $\{\mu_2\text{-}[\text{Fe}(\text{MeOH})_4]\text{-}\kappa^1\text{O-}[\text{Fe}(\eta^2\text{-O}_2\text{CO})(\text{rac-P4})]_2\}$ -  
710 (BPh<sub>4</sub>)<sub>2</sub> (**7'**).

711 **Reaction of 1 with K<sub>2</sub>CO<sub>3</sub>**. A 0.5 mL portion of a 0.01 M  
712 stock solution of **1** in PC were placed in a 5 mm NMR tube  
713 under argon. Solid K<sub>2</sub>CO<sub>3</sub> (7.0 mg, 0.05 mmol) was then  
714 added. The solution in the NMR tube was stirred with a small  
715 stirring bar, and the purple solution turned initially bright pink  
716 and then bright red. *d*<sub>8</sub>-Toluene (0.2 mL) was added for  
717 deuterium lock, and the red solution was analyzed by  $^{31}\text{P}\{^1\text{H}\}$   
718 NMR and  $^{13}\text{C}\{^1\text{H}\}$  NMR.  $^{31}\text{P}\{^1\text{H}\}$  NMR analysis showed  
719 formation of carbonate complex **7**, whereas no  $^{13}\text{C}\{^1\text{H}\}$  NMR  
720 resonance was observed for the carboxylic O<sub>2</sub>CO carbon of **7**.  
721  $^{31}\text{P}\{^1\text{H}\}$  NMR for **7** (PC + *d*<sub>8</sub>-toluene, 121.49 MHz):  $\delta_P$  105.1  
722 (t,  $^2J_{PP} = 30.4$  Hz; 2P, PPh), 69.0 (t,  $^2J_{PP} = 30.4$  Hz; 2P, PPh<sub>2</sub>).

723 **Reaction of 1 with FA under HPNMR Conditions and**  
724 **Formation of *cis*- $\alpha$ -[FeH(CO)(*rac*-P4)](BF<sub>4</sub>) (**9**)**. A 10 mm  
725 HPNMR sapphire tube was charged with a solution of  
726 Fe(BF<sub>4</sub>)<sub>2</sub>·6H<sub>2</sub>O (14 mg; 0.04 mmol) and *rac*-P4 (28 mg;  
727 0.04 mmol) in propylene carbonate (1.8 mL) under argon.  
728 CD<sub>3</sub>OD (0.4 mL) was then added for deuterium lock, followed  
729 by HCOOH (0.15 mL, 4.15 mmol; 100 equiv with respect to  
730 Fe). The tube was closed and placed in the NMR probe. The  
731 probe head was gradually heated to 60 °C, and the reaction was  
732 monitored by  $^{31}\text{P}\{^1\text{H}\}$  NMR (see the Supporting Information).  
733 The tube was left at 60 °C overnight, resulting in a yellow  
734 solution.  $^{31}\text{P}\{^1\text{H}\}$  and  $^1\text{H}$  NMR analysis revealed the  
735 quantitative formation of *cis*- $\alpha$ -[Fe(H)(CO)(*rac*-P4)](BF<sub>4</sub>)  
736 (**9**).  $^{31}\text{P}\{^1\text{H}\}$  NMR (121.49 MHz, CD<sub>3</sub>OD):  $\delta$  114.6 (dt,  $^2J_{PP}$   
737 = 23.5,  $^2J_{PP} = 38.6$ , 1P), 105.1 (br dd,  $^2J_{PP} = 8.6$ ,  $^2J_{PP} = 21.9$ ;  
738 1P), 100.9 (ddd,  $^2J_{PP} = 10.5$ ,  $^2J_{PP} = 39.3$ ,  $^2J_{PP} = 68.7$ ; 1P), 92.3  
739 (dd,  $^2J_{PP} = 37.9$ ,  $^2J_{PP} = 68.5$ ; 1P).  $^1\text{H}$  NMR (300.13 MHz,  
740 CD<sub>3</sub>OD, negative region):  $\delta$  -9.6 (ddd,  $^2J_{PP} = 25.5$ ,  $^2J_{PP} = 46.5$ ,  
741  $^2J_{PP} = 70.7$ ; 1H, FeH).  $^{13}\text{C}\{^1\text{H}\}$  NMR (75.47 MHz, CD<sub>3</sub>OD,  
742 carbonyl region):  $\delta$  162.77 (s; CO). A sharp singlet of higher  
743 intensity was also observed at  $\delta$  162.1 ppm for HCOOH. ESI-  
744 MS: calcd for  $^{12}\text{C}_{43}\text{H}_{43}\text{Fe}^{16}\text{O}^{31}\text{P}_4$  ([M]<sup>+</sup>) *m/z* 753.16550,  
745 found *m/z* 753.16517.

746 **Catalytic Tests. Catalytic Sodium Bicarbonate Hydro-**  
747 **genation Tests**. In a typical experiment, a 40 mL magnetically  
748 stirred stainless steel autoclave built at CNR-ICCOM was  
749 charged under an inert atmosphere (glovebox) with NaHCO<sub>3</sub>  
750 (typically 840 mg, 10 mmol) and the catalyst (0.01–0.001  
751 mmol as solid or stock solution in PC). The autoclave was then  
752 closed and thoroughly purged through several vacuum/argon  
753 cycles. MeOH (20.0 mL) was then added to the autoclave by  
754 suction. Finally the autoclave was pressurized with H<sub>2</sub> gas at the

desired pressure. The autoclave was then placed into an oil bath 755  
preheated to the desired temperature and stirred for the set 756  
reaction time. After the run, the autoclave was cooled in an ice/ 757  
water bath and depressurized, and the catalytic mixture was 758  
transferred to a flask and concentrated under vacuum at room 759  
temperature. The formate content was determined by analyzing 760  
aliquots (ca. 30 mg) of the solid mixture dissolved in D<sub>2</sub>O (0.5 761  
mL) by  $^1\text{H}$  NMR, using dry THF (20  $\mu\text{L}$ ) as internal standard 762  
with a relaxation delay of 20 s. 763

**Catalytic Formic Acid Dehydrogenation Tests**. In a typical 764  
experiment, a solution of catalyst (typically 5.3 mmol) in 765  
propylene carbonate (5 mL) was placed under an argon 766  
atmosphere in a magnetically stirred glass reaction vessel 767  
thermostated by external liquid circulation and connected to a 768  
reflux condenser and gas buret (2 mL scale). After the solution 769  
was heated to 40–60 °C, HCOOH (2.0 mL) was added and 770  
the experiment started. The gas evolution was monitored 771  
throughout the experiment by reading the values reached on 772  
the burets. The gas mixture was analyzed off-line by FTIR 773  
spectroscopy using a 10 cm gas-phase cell (KBr windows) to 774  
check for CO formation (detection limit 0.02%). 775

## ■ ASSOCIATED CONTENT

### 📄 Supporting Information

The following files are available free of charge on the ACS 778  
Publications website at DOI: 10.1021/cs501998t. 779

General methods and equipment, NMR spectra and 780  
details of HPNMR experiments, information on FA 781  
dehydrogenation tests, and details of the X-ray structure 782  
determinations ([PDF](#)) 783  
Crystallographic data for the X-ray crystal structure of **2** 784  
([CIF](#)) 785  
Crystallographic data for the X-ray crystal structure of **3**- 786  
BPh<sub>4</sub> ([CIF](#)) 787  
Crystallographic data for the X-ray crystal structure of **4** 788  
([CIF](#)) 789  
Crystallographic data for the X-ray crystal structure of **5** 790  
([CIF](#)) 791  
Crystallographic data for the X-ray crystal structure of **7'** 792  
([CIF](#)) 793

## ■ AUTHOR INFORMATION

### Corresponding Author

\*E-mail for L.G.: lgonsalvi@iccom.cnr.it. 796

### Notes

The authors declare no competing financial interest. 798

## ■ ACKNOWLEDGMENTS

Financial contributions by the CNR, MIUR, and ECRF 800  
through projects EFOR, Progetto Premiale 2012 “Integrated 801  
and eco-sustainable technologies for the production, storage 802  
and use of the energy”, and Firenze Hydrolab<sup>2</sup>, respectively, are 803  
gratefully acknowledged. This work was also supported by 804  
COST Action CM1205 CARISMA (Catalytic Routines for 805  
Small Molecule Activation). 806

## ■ REFERENCES

(1) (a) Turner, J. A. *Science* **2004**, *305*, 972–974. (b) Schlapbach, L.; 808  
Züttel, A. *Nature* **2001**, *414*, 353–358. (c) Armaroli, N.; Balzani, V. 809  
*Angew. Chem., Int. Ed.* **2007**, *46*, 52–66. (d) Lubitz, W. *Chem. Rev.* 810  
**2007**, *107*, 3900–3903. 811

- 812 (2) (a) Joó, F. *ChemSusChem* **2008**, *1*, 805–808. (b) Enthaler, S.  
813 *ChemSusChem* **2008**, *1*, 801–804. (c) Federsel, C.; Jackstell, R.; Beller,  
814 M. *Angew. Chem., Int. Ed.* **2010**, *49*, 6254–6257. (d) Loges, B.;  
815 Boddien, A.; Gärtner, F.; Junge, H.; Beller, M. *Top. Catal.* **2010**, *53*,  
816 902–914. (e) Enthaler, S.; Langermann, J.; Schmidt, T. *Energy Environ.*  
817 *Sci.* **2010**, *3*, 1207–1217.
- 818 (3) (a) Loges, B.; Boddien, A.; Junge, H.; Beller, M. *Angew. Chem.,*  
819 *Int. Ed.* **2008**, *47*, 3962–3965. (b) Boddien, A.; Loges, B.; Junge, H.;  
820 Beller, M. *ChemSusChem* **2008**, *1*, 751–758. (c) Boddien, A.; Loges,  
821 B.; Junge, H.; Gärtner, F.; Noyes, J. R.; Beller, M. *Adv. Synth. Catal.*  
822 **2009**, *351*, 2517–2520. (d) Junge, H.; Boddien, A.; Capitta, F.; Loges,  
823 B.; Noyes, J. R.; Gladiali, S.; Beller, M. *Tetrahedron Lett.* **2009**, *50*,  
824 1603–1606. (e) Boddien, A.; Gärtner, F.; Federsel, C.; Sponholz, P.;  
825 Mellmann, D.; Jackstell, R.; Junge, H.; Beller, M. *Angew. Chem., Int. Ed.*  
826 **2011**, *50*, 6411–6414. (f) Boddien, A.; Federsel, C.; Sponholz, P.;  
827 Mellmann, D.; Jackstell, R.; Junge, H.; Laurency, G.; Beller, M. *Energy*  
828 *Environ. Sci.* **2012**, 8907–8911. (g) Huff, C. A.; Sanford, M. S. *ACS*  
829 *Catal.* **2013**, *3*, 2412–2416.
- 830 (4) (a) Tanaka, R.; Yamashita, R.; Nozaki, K. *J. Am. Chem. Soc.* **2009**,  
831 *131*, 14168–14169. (b) Hull, J. F.; Himeda, Y.; Wang, W. H.;  
832 Hashiguchi, B.; Periana, R.; Szalda, D. J.; Fujita, E. *Nat. Chem.* **2010**, *4*,  
833 383–388. (c) Fukuzumi, S.; Kobayashi, T.; Suenobu, T. *J. Am. Chem.*  
834 *Soc.* **2010**, *132*, 1496–1497. (d) Himeda, Y. *Green Chem.* **2009**, *11*,  
835 2018–2022. (e) Himeda, Y.; Miyazawa, S.; Hirose, T. *ChemSusChem*  
836 **2011**, *4*, 487–493. (f) Himeda, Y.; Onozawa-Komatsuzaki, N.;  
837 Miyazawa, S.; Sugihara, H.; Hirose, T.; Kasuga, K. *Chem. Eur. J.*  
838 **2008**, *14*, 11076–11081. (g) Forster, D.; Beck, G. R. *Chem. Commun.*  
839 **1971**, 1072. (h) Coffey, R. S. *Chem. Commun.* **1967**, 923a–923a.
- 840 (5) (a) Federsel, C.; Boddien, A.; Jackstell, R.; Jennerjahn, R.; Dyson,  
841 P. J.; Scopelliti, R.; Laurency, G.; Beller, M. *Angew. Chem., Int. Ed.*  
842 **2010**, *49*, 9777–9780. (b) Boddien, A.; Gärtner, F.; Jackstell, R.;  
843 Junge, H.; Spannenberg, A.; Baumann, W.; Ludwig, R.; Beller, M.  
844 *Angew. Chem., Int. Ed.* **2010**, *49*, 8993–8996. (c) Boddien, A.; Loges,  
845 B.; Gärtner, F.; Toborg, C.; Fumino, K.; Junge, H.; Ludwig, R.; Beller,  
846 M. *J. Am. Chem. Soc.* **2010**, *132*, 8924–8934. (d) Langer, R.; Diskin-  
847 Posner, Y.; Leitus, G.; Shimon, L. J. W.; Ben-David, Y.; Milstein, D.  
848 *Angew. Chem., Int. Ed.* **2011**, *50*, 9948–9952. (e) Boddien, A.;  
849 Mellmann, D.; Gärtner, F.; Jackstell, R.; Junge, H.; Dyson, P. J.;  
850 Laurency, G.; Ludwig, R.; Beller, M. *Science* **2011**, *333*, 1733–1736.  
851 (f) Ziebart, C.; Federsel, C.; Anbarasan, P.; Jackstell, R.; Baumann, W.;  
852 Spannenberg, A.; Beller, M. *J. Am. Chem. Soc.* **2012**, *134*, 20701–  
853 20704. (g) Sánchez-de-Armas, R.; Xue, L.; Ahlquist, M. S. G. *Chem.*  
854 *Eur. J.* **2013**, *19*, 11869–11873. (h) Yang, X. *Dalton Trans.* **2013**, *42*,  
855 11987–11991.
- 856 (6) (a) Federsel, C.; Ziebart, C.; Jackstell, R.; Baumann, W.; Beller,  
857 M. *Chem. Eur. J.* **2012**, *18*, 72–75. (b) Jeletic, M. S.; Mock, M. T.;  
858 Appel, A. M.; Linehan, J. C. *J. Am. Chem. Soc.* **2013**, *135*, 11533–  
859 11536.
- 860 (7) The iron-catalyzed decomposition of formic acid by  $[\text{FeH}(\eta^2\text{-H}_2)$   
861  $(\text{PP}_3)]\text{BPh}_4$  was briefly reported in earlier literature; see: Bianchini, C.;  
862 Peruzzini, M.; Polo, A.; Vacca, A.; Zanobini, F. *Gazz. Chim. Ital.* **1991**,  
863 *121*, 543–549. Another highly active Fe-pincer based system,  
864 however, needing Lewis acids and higher temperatures (80 °C) to  
865 reach a TON of ca.  $10^6$ , was reported recently; see: Bielinski, E. A.;  
866 Lagaditis, P. O.; Zhang, Y.; Mercado, B. Q.; Würtele, C.; Bernskoetter,  
867 W. H.; Hazari, N.; Schneider, S. J. *J. Am. Chem. Soc.* **2014**, *136*, 10234–  
868 10237.
- 869 (8) These hydrides were originally described by: Bianchini, C.;  
870 Laschi, F.; Peruzzini, M.; Ottaviani, M. F.; Vacca, A.; Zanello, P. *Inorg.*  
871 *Chem.* **1990**, *29*, 3394–3402.
- 872 (9) (a) Mellone, I.; Peruzzini, M.; Rosi, L.; Mellmann, D.; Junge, H.;  
873 Beller, M.; Gonsalvi, L. *Dalton Trans.* **2013**, *42*, 2495–2501.  
874 (b) Manca, G.; Mellone, I.; Bertini, F.; Peruzzini, M.; Rosi, L.;  
875 Mellmann, D.; Junge, H.; Beller, M.; Ienco, A.; Gonsalvi, L.  
876 *Organometallics* **2013**, *32*, 7053–7064. (c) Bosquain, S. S.; Dorcier,  
877 A.; Dyson, P. J.; Erlandsson, M.; Gonsalvi, L.; Laurency, G.; Peruzzini,  
878 M. *Appl. Organomet. Chem.* **2007**, *21*, 947–951.
- (10) Erlandsson, M.; Landaeta, V. R.; Gonsalvi, L.; Peruzzini, M.; 879  
Phillips, A. D.; Dyson, P. J.; Laurency, G. *Eur. J. Inorg. Chem.* **2008**, *4*, 880  
620–627. 881
- (11) Brown, J. M.; Canning, L. R. *J. Organomet. Chem.* **1984**, *267*, 882  
179–190. 883
- (12) Bautista, M. T.; Earl, K. A.; Maltby, P. A.; Morris, R. H.; 884  
Schweitzer, C. T. *Can. J. Chem.* **1994**, *72*, 547–560. 885
- (13) King, R. B.; Heckley, P. R.; Cloyd, J. C., Jr. *Z. Naturforsch., B* 886  
**1974**, *296*, 574–575. 887
- (14) Bautista, M. T.; Earl, K. A.; Maltby, P. A.; Morris, R. H. *J. Am.* 888  
*Chem. Soc.* **1988**, *110*, 4056–4057. 889
- (15) King, R. B.; Kapoor, P. N. *J. Am. Chem. Soc.* **1969**, *91*, 5191– 890  
5192. 891
- (16) (a) King, R. B.; Kapoor, R. N.; Saran, M. S.; Kapoor, P. N. *Inorg.* 892  
*Chem.* **1971**, *10*, 1851–1860. (b) King, R. B.; Kapoor, P. N. *J. Am.* 893  
*Chem. Soc.* **1971**, *93*, 4112–4119, 4158–4166. (c) Ghilardi, C. A.; 894  
Midollini, S.; Stoppioni, P.; Sacconi, L. *Inorg. Chem.* **1973**, *12*, 1801– 895  
1805. (d) Bacci, M.; Ghilardi, C. A. *Inorg. Chem.* **1974**, *13*, 2398–2403. 896  
(e) Ghilardi, C. A.; Midollini, S.; Sacconi, L.; Stoppioni, P. *J.* 897  
*Organomet. Chem.* **1981**, *205*, 193–202. (f) Bacci, M.; Ghilardi, C. A.; 898  
Orlandini, A. *Inorg. Chem.* **1984**, *23*, 2798–2802. (g) Brown, J. M.; 899  
Canning, L. R. *J. Organomet. Chem.* **1984**, *267*, 179–190. (h) Rivera, V. 900  
A.; De Gil, E. R.; Fontal, B. *Inorg. Chim. Acta* **1985**, *98*, 153–159. 901  
(i) Brüggeller, P. *Inorg. Chem.* **1990**, *29*, 1742–1750. (j) Goller, H.; 902  
Brüggeller, P. *Inorg. Chim. Acta* **1992**, *197*, 75–81. (k) Chen, J.-D.; 903  
Cotton, F. A.; Hong, B. *Inorg. Chem.* **1993**, *32*, 2343–2353. (l) Cotton, 904  
F. A.; Hong, B.; Shang, M.; Stanley, G. G. *Inorg. Chem.* **1993**, *32*, 905  
3620–3627. (m) Chen, J.-D.; Cotton, F. A.; Hong, B. *Inorg. Chem.* 906  
**1993**, *32*, 2343–2353. (n) Jia, G.; Lough, A. J.; Morris, R. H. *J.* 907  
*Organomet. Chem.* **1993**, *461*, 147–156. (o) Dillinger, K.; Oberhauser, 908  
W.; Bachmann, C.; Brüggeller, P. *Inorg. Chim. Acta* **1994**, *223*, 13–20. 909  
(p) Airey, A. L.; Swiegers, G. F.; Willis, A. C.; Wild, S. B. *J. Chem. Soc.,* 910  
*Chem. Commun.* **1995**, 693–694. (q) Oberhauser, W.; Bachmann, C.; 911  
Brüggeller, P. *Polyhedron* **1995**, *14*, 787–792. (r) Oberhauser, W.; 912  
Bachmann, C.; Brüggeller, P. *Polyhedron* **1996**, *15*, 2223–2230. 913
- (17) (a) Hathaway, B. J.; Holah, D. G.; Underhill, A. E. *J. Chem. Soc.* 914  
**1962**, 2444–2448. (b) Heintz, R. A.; Smith, J. A.; Szalav, P. S.; 915  
Weisgerber, A.; Dunbar, K. R. *Inorg. Synth.* **2004**, *33*, 75–78. 916
- (18) Beck, W.; Stinkel, K. *Chem. Rev.* **1988**, *88*, 1405–1421. 917
- (19) Mellmann, D.; Barsch, E.; Bauer, M.; Grabow, K.; Boddien, A.; 918  
Kammer, A.; Sponholz, P.; Bentrup, U.; Jackstell, R.; Junge, H.; 919  
Laurency, G.; Ludwig, R.; Beller, M. *Chem. Eur. J.* **2014**, *20*, 13589– 920  
13602. 921
- (20) Habeck, C. M.; Hoberg, C.; Peters, G.; Näther, C.; Tuzcek, F. 922  
*Organometallics* **2004**, *23*, 3252–3258. 923
- (21) It was shown that heterolytic hydrogen splitting to give metal 924  
hydrides can occur even without the need for added base. See for 925  
example: (a) Kubas, G. J. *Adv. Inorg. Chem.* **2004**, *56*, 127–178. 926  
(b) Schlaf, M.; Lough, A. J.; Maltby, P. A.; Morris, R. H. 927  
*Organometallics* **1996**, *15*, 2270–2278. 928
- (22) Field, D. L.; Lawrence, E. T.; Shaw, W. J.; Turner, P. *Inorg.* 929  
*Chem.* **2000**, *39*, 5632–5638. 930
- (23) (a) Allen, O. R.; Dalgarno, S. J.; Field, L. D. *Organometallics* 931  
**2008**, *27*, 3328–3330. (b) Allen, O. R.; Dalgarno, S. J.; Field, L. D.; 932  
Jensen, P.; Willis, A. D. *Organometallics* **2008**, *27*, 2092–2098. 933
- (24) For other examples on the reductive disproportionation of CO<sub>2</sub> 934  
catalyzed by iron complexes, see: (a) Antberg, M.; Frosin, K.-M.; 935  
Dahlenburg, L. *J. Organomet. Chem.* **1988**, *338*, 319–327. (b) Sadique, 936  
A. R.; Brennessel, W. W.; Holland, P. L. *Inorg. Chem.* **2008**, *47*, 784– 937  
786. 938
- (25) As the <sup>31</sup>P{<sup>1</sup>H} AA'XX' pattern of **8** does not allow us to 939  
discriminate between O<sub>h</sub> and TBP geometries, we tentatively propose 940  
that the corresponding signals may be due to the formation of either 941  
*cis-α*-[Fe(η<sup>1</sup>-O<sub>2</sub>COH)<sub>2</sub>(rac-P4)] or *cis-α*-[Fe(η<sup>2</sup>-O<sub>2</sub>COH)(rac-P4)]<sup>+</sup>. 942
- (26) Complex **7** was generated in solution by the reaction of **1** with 943  
K<sub>2</sub>CO<sub>3</sub> in PC/CD<sub>3</sub>OD (3:1) and then reacted with H<sub>2</sub> (30 bar) under 944  
HPNMR conditions. Slow conversion to **3-BF<sub>4</sub>** was observed to occur 945  
upon heating and standing at 60 °C. 946

947 (27) Gas mixture analyses were carried out by FTIR spectroscopic  
948 methods described in previous publications. For details see: (a) Morris,  
949 D. J.; Clarkson, G. J.; Wills, M. *Organometallics* **2009**, *28*, 4133–4140.  
950 (b) Guerriero, A.; Bricout, H.; Sordakis, K.; Peruzzini, M.; Monflier,  
951 E.; Hapiot, F.; Laurency, G.; Gonsalvi, L. *ACS Catal.* **2014**, *4*, 3002–  
952 3012.